

## **Section 5. Observations of the Earth's Atmosphere**

One of the most important applications of satellite measurements is remote sounding of atmospheric properties:

- profiles of temperature
- profiles of trace gas concentrations
- clouds
- aerosols
- precipitation
- winds
- pressure at a reference level
- sea surface temperature
- water vapour pressure

We will look at the measurement of temperature first as it provides a useful example of the inversion of the radiative transfer equation.

### **5.1 Measurements of Temperature**

#### ***References***

- *Kidder and Vonder Haar: chapter 6, pp. 183-196*
- *Stephens: chapter 7, pp. 356-364*
- *Houghton, Taylor, and Rodgers: chapter 5; chapter 6*
- *Liou: chapter 7, pp. 250-271, 280-285*

Monitoring of global temperature is important for studying climate change. e.g., current controversy between ground-based and satellite observations of temperature trends

*See figure (Harries 2.13) – temperature-altitude profile for Earth.*

The vertical profile of atmospheric temperature is used to define four regions of the atmosphere between 0 and 100 km:

- (1) troposphere – 0 to 10 km, T decreases with height
- (2) stratosphere – 10 to 50 km, T increases with height due to ozone layer
- (3) mesosphere – 50 to 90 km, T decreases with height again
- (4) thermosphere – above 90 km, T increases with height due to oxygen

These layers are separated by the tropopause, stratopause, and mesopause.

The lowest 1-2-3 km of the troposphere is the planetary boundary layer, where there are strong interactions with the surface and large diurnal variations.

Temperature sounding generally involves the detection of radiation emitted by a gas which is uniformly distributed in the atmosphere, so that the emission is a function of temperature only.

e.g., CO<sub>2</sub> at 4.3 μm at 15 μm  
O<sub>2</sub> at 60 GHz

### 5.1.1 Nadir Sounding of Temperature

#### Nadir viewing or vertical sounding

The satellite instrument looks vertically downwards in the [near] nadir direction, measuring radiation that leaves the atmosphere in the [near] local vertical.

- this viewing geometry provides a limited vertical resolution

Recall the solution to Schwarzschild's Equation (RTE for no scattering, valid in the IR):

$$I_{\lambda}(z_1) = I_{\lambda}(0)\tau_{\lambda}(0, z_1) + \int_{\text{surface} \rightarrow \tau_{\lambda}(0, z_1)}^{\text{satellite} \rightarrow \tau_{\lambda}(z_1, z_1)=1} B_{\lambda}(T) d\tau_{\lambda}$$

= surface radiance  $\times \tau$  from surface to satellite  
 + radiance emitted by each layer  $\times \tau$  from that layer to satellite

where

$$\tau_{\lambda}(z, z_1) = \exp\left[-\int_z^{z_1} \frac{k_a \rho}{\mu} dz\right] = \exp\left[-\int_{u(z)}^{u(z_1)} k_a du\right] = \text{transmission from } z \text{ to } z_1.$$

Now introduce an altitude-dependent variable  $y$ , which can be  $z$ ,  $p$ ,  $\ln(p)$ , or any function monotonic in  $z$ .

$$I_{\lambda}(z_1) = I_{\lambda}(0)\tau_{\lambda}(0, z_1) + \int_{\text{surface}}^{\text{satellite}} B_{\lambda}(T) \frac{d\tau_{\lambda}}{dy} dy$$

$$= I_{\lambda}(0)\tau_{\lambda}(0, z_1) + \int_{\text{surface}}^{\text{satellite}} B_{\lambda}(T) K_{\lambda}(y) dy$$

where

$$K_{\lambda}(y) = \frac{d\tau_{\lambda}}{dy} \text{ is called a weighting function .}$$

Often,  $y = -\ln(p)$  to make  $K_{\lambda}(y)$  more nearly independent of temperature.

A nadir-viewing instrument thus sees a surface term  $I_{\lambda}(0)\tau_{\lambda}(0, z_1)$ , and an atmospheric term which is the integral of the blackbody emission from each layer weighted by  $K_{\lambda}(y)$ .

We can determine the form of  $K_{\lambda}(y)$  by considering the lower atmosphere ( $< 40$  km) where Lorentz broadening dominates and the absorption coefficient is thus:

$$k_a = \frac{S}{\pi} \frac{\alpha_L}{(\bar{\nu} - \bar{\nu}_0)^2 + \alpha_L^2} = \frac{S}{\pi} \frac{\alpha'_L p}{(\bar{\nu} - \bar{\nu}_0)^2 + (\alpha'_L p)^2}$$

where

$$\alpha_L(T, p) = \alpha_L^0(T_0, p_0) \frac{p}{p_0} \sqrt{\frac{T_0}{T}} \text{ and } \alpha'_L = \frac{\alpha_L(T, p)}{p} = \alpha_L^0(T_0, p_0) \frac{1}{p_0} \sqrt{\frac{T_0}{T}} .$$

Note: now working in  $\bar{v}$  space rather than  $\lambda$  space.

In the far wings of the Lorentz line, where  $\bar{v} - \bar{v}_o \gg \alpha'_L p$ :  $k_a \approx \frac{S}{\pi} \frac{\alpha'_L p}{(\bar{v} - \bar{v}_o)^2}$ .

Thus, the transmission becomes

$$\begin{aligned} \tau_{\bar{v}}(z, z_1) &= \exp \left[ - \int_{u(z)}^{u(z_1)} k_a du \right] \\ &= \exp \left[ - \int_{p(z)}^{p(z_1)} k_a \left( - \frac{Q}{\mu g} \right) dp \right] \\ &= \exp \left[ \frac{Q}{\mu g} \int_p^{p(z_1)=0} k_a dp \right] \\ &= \exp \left[ \frac{Q}{\mu g} \int_p^0 \frac{S}{\pi} \frac{\alpha'_L p}{(\bar{v} - \bar{v}_o)^2} dp \right] \\ &= \exp \left[ \frac{QS\alpha'_L}{\pi\mu g(\bar{v} - \bar{v}_o)^2} \int_p^0 p dp \right] \\ &= \exp[-Ap^2] \end{aligned}$$

where

$$A \equiv \frac{QS\alpha'_L}{2\pi\mu g(\bar{v} - \bar{v}_o)^2}$$

and we have used the hydrostatic equation as follows

$$du = \rho_{\text{gas}} ds = \rho_{\text{gas}} \frac{dz}{\mu} = \frac{1}{\mu} \rho_{\text{gas}} dz = \frac{1}{\mu} \rho_{\text{gas}} \left( - \frac{dp}{\rho_{\text{air}} g} \right) = \frac{1}{\mu} \left( - \frac{Q}{g} dp \right)$$

with

$$Q = \frac{\rho_{\text{gas}}}{\rho_{\text{air}}} = \text{mass mixing ratio, assumed constant for a well-mixed gas.}$$

Now the weighting function can be determined

$$K_{\bar{v}}(y) = \frac{d\tau_{\bar{v}}}{dy} = -p \frac{d\tau_{\bar{v}}}{dp} = -p(-2Ap) \exp[-Ap^2] = 2Ap^2 \exp[-Ap^2]$$

using  $y = -\ln(p)$ ,  $dy = -dp/p$ .

Where (at what  $p_{\max}$ ) does the weighting function have a maximum?

$$\frac{dK_{\bar{v}}}{dy} = 0 = 2A \left\{ 2p_{\max} \exp[-Ap_{\max}^2] + p_{\max}^2 (-2Ap_{\max}) \exp[-Ap_{\max}^2] \right\}$$

$$2p_{\max} + p_{\max}^2 (-2Ap_{\max}) = 0$$

$$p_{\max} = \frac{1}{\sqrt{A}}$$

$$\text{So } K_{\bar{v}}(p) = 2 \left( \frac{p}{p_{\max}} \right)^2 \exp \left[ - \left( \frac{p}{p_{\max}} \right)^2 \right].$$

We can plot  $K_{\bar{v}}(p)$  vs.  $\frac{p}{p_{\max}}$ .

*See figure (Houghton 12.5) – three weighting functions*

Comments:

The value of  $p_{\max}$ , i.e., the height of the maximum value of  $K_{\bar{v}}(p)$ , depends on  $\bar{v}$ .

However, the half-width of the curve in units of  $\ln(p)$  is independent of  $\bar{v}$ . If the atmosphere were isothermal (at constant  $T$ ), then this half-width would be  $\sim 10$  km and would define the best possible vertical resolution.

Now, how is the weighting function applied to obtain a vertical profile of temperature?

Because  $k_a$  and  $K_{\bar{v}}$  vary with  $\bar{v}$ , different  $\bar{v}$  will possess weighting functions that peak at different heights. By measuring the intensities at a series of  $\bar{v}$ , a range of altitudes will be represented. Observations in the wings of a Lorentz line will see deeper into the atmosphere, while observations closer to line centre will see only the top layers of the atmosphere.

*See figures (Houghton 12.6 = H,T,&R 5.4, Liou 7.5) – examples of thermal emission spectra. In (a) radiation from the Q branch at the centre of the CO<sub>2</sub> band at 667 cm<sup>-1</sup> originates at temperatures approaching 240 K, well within the stratosphere. At higher wavenumbers, the absorption coefficient decreases and the brightness temperature falls to 220 K, which is characteristic of the tropopause. It then rises steadily as the peak of the appropriate weighting function falls in altitude until 800 cm<sup>-1</sup>, at which point most of the radiation comes from the surface. In contrast, (c) shows Antarctica, where the temperature throughout the troposphere and stratosphere increases with altitude from about 185 K at the surface to 220 K in the stratosphere.*

In practice, most radiometers measure the intensity with a spectral bandwidth much broader than that of a single line, and so the weighting functions are effectively smeared out over several layers (e.g. curve 'c' in figure 12.5 of Houghton).

Returning to the measured intensity: 
$$I_{\bar{\nu}}(z_1) = I_{\bar{\nu}}(0)\tau_{\bar{\nu}}(0, z_1) + \int_{\text{surface}}^{\text{satellite}} B_{\bar{\nu}}(T)K_{\bar{\nu}}(y)dy$$

The contribution of the surface emission term  $I_{\bar{\nu}}(0)\tau_{\bar{\nu}}(0, z_1)$  will be reduced if the transmission is small, i.e., if the observation is NOT being made in an atmospheric window.

The atmospheric emission term includes information on the temperature through the blackbody function, and on both the temperature and the concentration profile of the absorbing/emitting gas through the transmission and hence through the weighting function.

For temperature retrievals, we want to observe the intensity for an absorbing gas which

- is well mixed in the atmosphere (has a constant mixing ratio)
- has well known absorption lines

Preferred regions (both gases are well mixed up to ~90 km):

- (1) CO<sub>2</sub> near 15 μm
- (2) O<sub>2</sub> near 60 GHz (5 mm)

### **5.1.2 Limb Sounding of Temperature**

#### Limb viewing or sounding

The satellite instrument looks towards the limb (horizon) of the atmosphere, measuring radiation that leaves the atmosphere nearly tangentially.

Advantages and disadvantages are discussed below.

*See figure (Liou 7.8) - the geometry of limb viewing.*

For limb viewing observations, the same radiative transfer equation is used, but for a different geometry:

- no longer have a surface term
- the intensity is integrated along the limb viewing line-of-sight

The appropriate RTE, again assuming a non-scattering case, is

$$I_{\bar{\nu}}(z_{\text{tangent}}) = \int_{-\infty}^{\infty} B_{\bar{\nu}}[T(x)] \frac{\tau_{\bar{\nu}}(x, z_{\text{tangent}})}{dx} dx$$

where

$z_{\text{tangent}}$  = tangent height, the height above the surface of the closest point to the Earth in the instrument's line-of-sight

$x$  = distance along the line-of-sight (or ray path) with the origin at the tangent point

Since the temperature profile is wanted as a function of  $z$ , not  $x$ , this equation is converted to a vertical integral

$$I_{\bar{\nu}}(z_{\text{tangent}}) = \int_{z_{\text{tangent}}}^{z_1=\infty} B_{\bar{\nu}} [T(z)] K_{\bar{\nu}}(z, z_{\text{tangent}}) dz$$

where

$$K_{\bar{\nu}}(z, z_{\text{tangent}}) = \left[ \left( \frac{d\tau_{\bar{\nu}}(x, z_{\text{tangent}})}{dx} \right)_{+} + \left( \frac{d\tau_{\bar{\nu}}(x, z_{\text{tangent}})}{dx} \right)_{-} \right] \frac{dx}{dz}$$

+/- indicate values along the +x and -x directions.

See figure (Liou 7.9) - limb viewing weighting functions

→ note the sharp cut-off at the lower boundary because the atmosphere is not viewed below the tangent height

Advantages of limb sounding:

- (1) Good vertical resolution because the weighting functions peak sharply at the tangent height, with the instrument seeing nothing below  $z_{\text{tangent}}$  while pressure and density decrease exponentially above  $z_{\text{tangent}}$ .
- (2) The background is either the direct source (Sun) or space (which is cold and uniform) unlike the hot and variable surface of the Earth.
- (3) There is as much as 60-75 more emitting/absorbing material in the limb path than along the nadir path, allowing measurements of temperature and composition to higher altitudes and measurements of gases having lower concentrations

Disadvantages of limb sounding:

- (1) Observations are limited to the upper troposphere and above, due to clouds and the finite [2 km ?] field-of-view of the instrument.
- (2) The horizontal resolution is low.
- (3) It requires precise information about the field-of-view and spacecraft attitude so that the spacecraft pointing can be accurately determined.

### **5.1.3 Retrieval Methods**

We will only discuss these in general terms, as full solutions generally involve use of computers, etc..

So far, we have discussed the RTE that applies to nadir and limb sounding of temperature, and we have introduced the concept of a weighting function.

Now, we will address the retrieval problem: how is the temperature profile derived from the measured radiances  $I_{\bar{\nu}}$  at a series of  $\bar{\nu}$  ?

Even under cloud-free conditions, with a noise-free radiometer that measures radiances at all  $\bar{\nu}$  or  $\lambda$ , a unique solution for  $T(z)$  is not guaranteed. With noise and a limited number of  $\bar{\nu}$ , an infinite number of solutions is possible.

The problem is to find a temperature profile that satisfies the RTE and approximates the true profile as closely as possible.

Many approaches have been used to solve the retrieval problem. They can be roughly grouped into three categories.

#### **(1) Physical Retrievals**

These use the forward calculation in an iterative process.

- i) A first guess (*a priori*) temperature profile is chosen.
- ii) Weighting functions are calculated.
- iii) The forward problem (RTE) is solved for the radiance at each  $\bar{\nu}$ .
- iv) If the calculated radiances match the observed radiances within the noise level of the radiometer, then the current profile is accepted.
- v) If the calculated and observed radiances do not agree, then the current profile is adjusted and the above steps are repeated.

Advantages:

- physical processes are clear at each stage of the retrieval
- no large database of coincident radiosonde data is needed

Disadvantages:

- computationally expensive
- require accurate knowledge of the transmittances
- do not use known statistical properties of the atmosphere (except in first guess)

Examples:

### Chahine's Method

This is a widely used inversion technique that retrieves temperature for as many levels as there are channels (wavelengths) in the radiometer, say  $m$ . Each temperature corresponds to the peak of the weighting function for a channel. Thus, there is a one-to-one correspondence between channel  $i$  and the temperature at level  $i$  where the weighting function of channel  $i$  peaks.

For a temperature retrieval, the iteration is done through the Planck function, for one level at a time.

Let  $T_i^k$  = the  $k^{\text{th}}$  estimate of the temperature at level  $i$

$B_i(T_i^k)$  = the corresponding Planck blackbody radiance at level  $i$  and at  $\lambda$  of channel  $i$

$I_i^k(T_i^k)$  =  $k^{\text{th}}$  estimate of the radiance in channel  $i$ , calculated using the RTE for  $T_i^k$

$\tilde{T}_i$  = the measured radiance in channel  $i$

Then the Planck blackbody radiance is iterated using:  $B_i(T_i^{k+1}) = B_i(T_i^k) \frac{\tilde{T}_i}{I_i^k(T_i^k)}$

With this approach:

- a first guess temperature  $T_i^0$  is chosen for level  $i$
- $I_i^0(T_i^0)$  is calculated using the RTE, and  $B_i(T_i^0)$  is calculated using the Planck function
- the iterated Planck blackbody radiance  $B_i(T_i^1)$  is obtained using the above equation (and the measured radiance  $\tilde{T}_i$ )
- the iterated temperature  $T_i^1$  is derived from the “inverse Planck function”
- these steps are repeated until the simulated,  $I_i^{k+1}(T_i^{k+1})$ , and measured,  $\tilde{T}_i$ , radiances agree within some defined limit  
→  $T_i^{k+1}$  is then the best estimate of the temperature at level  $i$

This approach works because:

- if the calculated radiance is greater than the measured radiance, then the Planck radiance and hence the temperature will be adjusted downwards, and vice versa
- using the ratio of the observed to calculated radiance to adjust the Planck radiance is valid since the peak of the weighting function at level  $i$  makes the largest contribution to the radiance measured in channel  $i$

## Smith's Method

This is also widely used and is similar to Chahine's method. The difference is that the retrieval of temperature is not restricted to be at the same number of levels as there are channels, nor to be at the peaks of the weighting functions. This is a more flexible scheme since the number and height of levels can be chosen, but there will still only be  $m$  independent temperatures if there are  $m$  channels; temperatures retrieved at more than  $m$  levels will not be independent.

Given that an instrument has  $m$  channels (i.e.,  $m$  measurements are made) and that the temperature is to be retrieved on  $n$  levels.

Let  $T_j^k$  = the  $k^{\text{th}}$  estimate of the temperature at level  $j$

$B_i(T_j^k)$  = the corresponding Planck blackbody radiance at level  $j$  and for channel  $i$

$I_i^k(T_j^k)$  =  $k^{\text{th}}$  estimate of the radiance in channel  $i$ , calculated using the RTE for  $T_j^k$

$\tilde{T}_i$  = the measured radiance in channel  $i$

At each level  $j$ ,  $m$  estimates of the iterated Planck blackbody radiance are obtained using:

$$B_i(T_{ij}^{k+1}) = B_i(T_j^k) + [\tilde{T}_i - I_i^k(T_j^k)]$$

The  $m$  estimates of the iterated temperature at level  $j$  ( $T_j^{k+1}$ ), denoted by  $T_{ij}^{k+1}$ , are derived from the inverse Planck function. The "goodness" of each of these  $m$  estimates varies because each channel has a different weighting function and is more sensitive to certain levels.

Using Smith's Method, the solution for temperature  $T_j^{k+1}$  is calculated as a weighted average of the  $m$  estimates, with the weighting functions serving as the weights:

$$T_j^{k+1} = \frac{\sum_{i=1}^m K_{ij} T_{ij}^{k+1}}{\sum_{i=1}^m K_{ij}}$$

With this approach, the temperature at a particular level  $j$  cannot be obtained using only the measurement in a single channel because the levels are not necessarily at the peaks of the weighting functions.

Instead, a solution for the temperature at level  $j$  is obtained from every channel and the weighting functions are used to combine these estimates into a single solution for  $T_j$ .

This procedure is repeated for all  $n$  levels, to build up a vertical profile of temperature.

## (2) Statistical Retrievals

These do not use the RTE directly. Instead, they rely on statistical relationships between ground- and space-based measurements.

- i) A training data set of radiosonde temperature profile soundings nearly coincident in time and space with the satellite soundings is compiled.
- ii) This data set is used to calculate a statistical relationship between the satellite radiances and the radiosonde temperatures.
- iii) These relationships are then applied to other radiances to retrieve temperature profiles.

Advantages:

- computationally easy, which makes these useful for operational retrievals that must process many radiance measurements
- require no knowledge of the transmittances nor use of the RTE
- extensively use known statistical properties of the atmosphere

Disadvantages:

- a large database of coincident radiosonde data is needed for each satellite instrument → should cover all seasons, times of day, latitudes, longitudes, surface types (land, ocean, etc.), and view an area at the same time as the satellite
- physical processes are embedded in the statistics  
e.g., few radiosondes are launched from high (ground) elevations, so training data sets provide poor coverage of such regions potentially leading to biases in the retrievals

## (3) Hybrid Retrievals (or Inverse Matrix Methods)

These combine elements of physical and statistical retrievals. They do not require a large training data set and do use weighting functions.

- i) The RTE is first linearized about a standard temperature profile and is converted into a matrix equation.
- ii) This equation is used to obtain a matrix relating the temperature profile to the radiances, and including the weighting functions.
- iii) Then several possible approaches can be taken to solve the problem.

Advantages:

- easier to implement than physical or statistical methods
- include known statistical properties of the atmosphere
- no large database of coincident radiosonde data is needed

Disadvantages:

- require accurate knowledge of the transmittances

## Optimal Estimation – an example of a hybrid retrieval method

One approach to the retrieval of vertical profiles is the method of optimal estimation, sometimes called the minimum variance or the maximum likelihood method.

The formulation of Rodgers

(*Rev. Geophys. and Space Phys.*, **14**, 609, 1976; and *J. Geophys. Res.*, **95**, 5587, 1990):

- has general applicability
- provides an elegant method of combining *a priori* information with measurements
- explicitly calculates error on a retrieved profile from the errors in these quantities

The retrieval and characterization of the system start with the definition of a forward model F

$$\mathbf{y} = F(\mathbf{x}, \mathbf{b}) + \boldsymbol{\varepsilon}$$

where

$\mathbf{y}$  = vector of m measurements

(e.g. nadir radiances in m channels limb radiances obtained at m tangent heights)

$\mathbf{x}$  = atmospheric profile defined at n levels (e.g. temperature or gas concentration)

$\mathbf{b}$  = vector of model parameters

$\boldsymbol{\varepsilon}$  = vector of measurement errors, assumed to be normally distributed about zero with error covariance matrix  $\mathbf{S}_y$  which expresses the correlated errors between measurements

Note: Bold case is used to denote vectors and matrices.

The forward model is used to calculate the weighting function matrix:  $\mathbf{K} = \frac{\partial F}{\partial \mathbf{x}}$ .

$\mathbf{K}$  can be derived analytically or by perturbing each element of  $\mathbf{x}$  in turn, and calculating the resulting perturbations in each element of  $\mathbf{y}$ .

The rows of  $\mathbf{K}$  are the weighting functions

→ illustrate region of the profile that is represented by each measurement

Then, given a set of measurements  $\mathbf{y}$ , the profile  $\hat{\mathbf{x}}$  and its covariance  $\hat{\mathbf{S}}$  can be retrieved using the optimal estimation equations

$$\hat{\mathbf{x}} = \mathbf{x}_o + \mathbf{S}_o \mathbf{K}^T (\mathbf{K} \mathbf{S}_o \mathbf{K}^T + \mathbf{S}_y)^{-1} (\mathbf{y} - \mathbf{K} \mathbf{x}_o)$$

$$\hat{\mathbf{S}} = \mathbf{S}_o - \mathbf{S}_o \mathbf{K}^T (\mathbf{K} \mathbf{S}_o \mathbf{K}^T + \mathbf{S}_y)^{-1} \mathbf{K} \mathbf{S}_o$$

where

$\mathbf{x}_o$  is the *a priori* estimate of the true profile  $\mathbf{x}$

$\mathbf{S}_o$  is its error covariance

These equations combine the virtual measurement obtained from the *a priori* information with the real measurements to give the best estimate of the profile and its covariance. In practice, these equations are solved sequentially, using each scalar measurement  $y_i$ , in turn, to improve the estimate of  $\hat{\mathbf{x}}$  from the initial guess through m intermediate values to the final solution.

How are these equations derived?

Assume there are only two independent measurements  $x_1$  and  $x_2$  of some scalar  $x$ . Then  $x$  can be “retrieved” as the weighted average of these two quantities:

$$\hat{x} = \left( \frac{1}{\frac{1}{\sigma_1^2} + \frac{1}{\sigma_2^2}} \right) \left( \frac{x_1}{\sigma_1^2} + \frac{x_2}{\sigma_2^2} \right) \quad \text{with variance} \quad \hat{\sigma}^2 = \left( \frac{1}{\frac{1}{\sigma_1^2} + \frac{1}{\sigma_2^2}} \right).$$

This can be generalized to vectors, replacing  $x$  by  $\mathbf{x}$  and  $\sigma$  by  $\mathbf{S}$ , so

$$\hat{\mathbf{x}} = \left( \frac{1}{\mathbf{S}_1^{-1} + \mathbf{S}_2^{-1}} \right) (\mathbf{S}_1^{-1} \mathbf{x}_1 + \mathbf{S}_2^{-1} \mathbf{x}_2).$$

Then, given a priori estimate  $\mathbf{x}_o$  with error covariance  $\mathbf{S}_o$ , and measurement  $\mathbf{y} = \mathbf{K}\mathbf{x}$  with error covariance  $\mathbf{S}_y$ , this equation becomes

$$\hat{\mathbf{x}} = \left( \frac{1}{\mathbf{S}_x^{-1} + \mathbf{K}^T \mathbf{S}_y^{-1} \mathbf{K}} \right) (\mathbf{S}_x^{-1} \mathbf{x}_o + \mathbf{K}^T \mathbf{S}_y^{-1} \mathbf{y}).$$

With some rearrangement, this equation for  $\hat{\mathbf{x}}$  and that for  $\hat{\mathbf{S}}$  can be converted to the forms above.

An Aside: Definition of covariance

Recall the definition of standard deviation:  $\sigma = \sqrt{\frac{1}{N-1} \sum_{i=1}^N (x_i - \bar{x})^2}$

This represents the root-mean-square (RMS) deviation of a set of  $N$  data points  $x_i$  from the mean  $\bar{x}$ . The variance is defined as  $\sigma^2$ .

Given a vector of data points,  $\mathbf{x}$ , there will be a corresponding vector  $\sigma$  or  $\sigma^2$ . It is customary to use the variance and to use a matrix rather than a vector, with the variances comprising the diagonal elements of this covariance matrix.

The elements of this matrix are the covariance elements, formally defined as:

$$S_{jk} = \frac{1}{\sum_{i=1}^N \frac{X_j(x_i) X_k(x_i)}{\sigma_i^2}} \quad \text{where } X_j \text{ and } X_k \text{ are some functions of } x_i.$$

Alternatively, using the expectation symbol  $E\{x\}$  which is like a summation over many instances of a random variable, we can write

$$\mathbf{S}_y = E\{\boldsymbol{\varepsilon} \boldsymbol{\varepsilon}^T\} = E\{[\mathbf{y} - \mathbf{F}(\mathbf{x})][\mathbf{y} - \mathbf{F}(\mathbf{x})]^T\}$$

$$\mathbf{S}_o = E\{(\mathbf{x}_o - \mathbf{x})(\mathbf{x}_o - \mathbf{x})^T\} \quad \text{and} \quad \hat{\mathbf{S}} = E\{(\hat{\mathbf{x}} - \mathbf{x})(\hat{\mathbf{x}} - \mathbf{x})^T\}$$

See Press et al., *Numerical Recipes, Chapters 15 and 18* for a discussion of covariance.

Returning to optimal estimation...

The retrieved profile  $\hat{\mathbf{x}}$  can be related to the real profile  $\mathbf{x}$  using

$$\hat{\mathbf{x}} = \mathbf{l}(\mathbf{y}) = \mathbf{l}(\mathbf{F}(\mathbf{x})) = \mathbf{T}(\mathbf{x})$$

where

$\mathbf{l}(\mathbf{y}, \mathbf{b}, \mathbf{c}) =$  inverse model defining  $\hat{\mathbf{x}}$  in terms of  $\mathbf{y}$

$\mathbf{c}$  = vector of parameters that are used in the retrieval

$\mathbf{T}$  = transfer function relating  $\hat{\mathbf{x}}$  to  $\mathbf{x}$ .

The matrix of averaging kernels is then defined as  $\mathbf{A} = \frac{d\mathbf{T}}{d\mathbf{x}} = \frac{d\mathbf{l}}{d\mathbf{y}} \frac{d\mathbf{F}}{d\mathbf{x}} = \mathbf{D}\mathbf{K}$

where  $\mathbf{D} = \frac{\partial \mathbf{l}}{\partial \mathbf{y}}$  = matrix of contribution functions.

Each column of  $\mathbf{D}$  represents the contribution to the solution due to a unit change in the corresponding element of  $\mathbf{y}$ .

$\hat{\mathbf{x}}$  at a given altitude = average of real profile  $\mathbf{x}$  weighted by the corresponding row of  $\mathbf{A}$

The width of the primary peaks of the averaging kernels is a qualitative measure of the vertical resolution.

*See figures – optimal estimation calculations for OSIRIS.*

#### **5.1.4 Temperature-Sounding Satellite Instruments**

These are generally radiometers or spectrometers that include

- an optical system that defines the field-of-view and collects the radiation
- another optical system that defines the spectral channels
- a detector

##### **A selection of instruments:**

(1) Medium Resolution Infrared Radiometer (MRIR)

- first satellite instrument to measure temperature
- flew on TIROS 7 satellite in 1963
- filter radiometer that used a single channel at 15  $\mu\text{m}$  for temperature sounding
- measured a single temperature for the lower stratosphere, centered on 20 km

(2) Satellite Infrared Spectrometer (SIRS)

- first instrument to measure temperature with extended vertical coverage
- flew on Nimbus 3 (1969) and Nimbus 4 (1970)
- grating spectrometer with eight channels 5  $\text{cm}^{-1}$  wide in the 15  $\mu\text{m}$   $\text{CO}_2$  band
- covered 0 to 35 km

### (3) Infrared Interferometer Spectrometer (IRIS)

- also flew on Nimbus 3 and 4
- Michelson interferometer which recorded the spectrum from 5-25  $\mu\text{m}$  at  $5\text{ cm}^{-1}$  resolution
- used the 15  $\mu\text{m}$   $\text{CO}_2$  band for the temperature profile retrieval

### (4) Other IR (15 $\mu\text{m}$ $\text{CO}_2$ ) multichannel filter radiometers

- ITPR – Infrared Temperature Profile Radiometer
- HIRS – High Resolution Infrared Radiation Sounder
- VTPR – Vertical Temperature Profile Radiometer
- VISSR – Visible Infrared Spin Scan Radiometer (geostationary orbit)
- SCR – Selective Chopper Radiometer
- PMR – Pressure Modulator Radiometer

### (5) Microwave instruments

- NEMS – Nimbus E Microwave Spectrometer (1972) had three channels in the 5 mm  $\text{O}_2$  band to retrieve temperatures up to 20 km
- SCAMS – Scanning Microwave Spectrometer
- MSU – Microwave Sounding Unit
- AMSU – Advanced MSU

### (6) Limb-sounding instruments

#### LRIR – Limb Sounding Infrared Radiometer

- first limb sounding IR radiometer to observe the atmosphere
- flew on Nimbus 6 in 1975
- four channel filter radiometer with two channels in the 15  $\mu\text{m}$   $\text{CO}_2$  band
- provided 1-2 km vertical resolution

#### LIMS – Limb Infrared Monitor of the Stratosphere

- flew on Nimbus 7 in 1978
- six channel with two in the 15  $\mu\text{m}$   $\text{CO}_2$  band
- measured temperature profiles up to 65 km

#### SAMS – Stratospheric and Mesospheric Sounder

- flew on Nimbus 7 in 1978
- used six pressure modulated cells as filters with one for temperature

### (7) Current operational temperature sounders

- TOVS – TIROS N Operational Vertical Sounder, flown on the NOAA LEO satellites, consists of three instruments  
HIRS/2 – High Resolution Infrared Radiation Sounder  
MSU – Microwave Sounding Unit  
SSU – Stratospheric Sounding Unit)
- VISSR – Visible and Infrared Spin Scan Radiometer, flown on GOES geostationary satellites since 1987

## **5.2 Measurements of Atmospheric Composition**

### ***References***

- *Kidder and Vonder Haar: chapter 6, pp. 210-218*
- *Stephens: chapter 6, pp. 271-278, 294-298, 302-304; chapter 7, pp. 328-331, 356-364*
- *Houghton, Taylor, and Rodgers: chapter 10*
- *Liou: chapter 7, pp. 236-242, 246-250*
- *Lenoble: chapter 23, pp. 454-461; chapter 24, chapter 25, pp. 490-498*

The general principles for remote sounding of atmospheric composition are the same as those for remote sounding of temperature. Both use the fact that at any  $\lambda$  or  $\bar{\nu}$ , atmospheric transmission is a function of the temperature and of the mixing ratio of any gas that absorbs radiation at that  $\lambda$  or  $\bar{\nu}$ .

Two approaches:

- (1) For a well-mixed gas (e.g., CO<sub>2</sub>, O<sub>2</sub>):
  - mixing ratio is known and constant with height
  - can retrieve temperature from measurements of  $I(\lambda)$  at  $\lambda$  where the gas absorbs
- (2) For a gas whose mixing ratio varies with altitude (e.g., O<sub>3</sub>, H<sub>2</sub>O):
  - assume a temperature profile
  - can retrieve mixing ratio from measurements of  $I(\lambda)$  at  $\lambda$  where the gas absorbs

Which gases are measured?

The three most important minor constituents are O<sub>3</sub>, CO<sub>2</sub>, and H<sub>2</sub>O. All have a role in determining atmospheric temperature structure and energy balance because they absorb solar and terrestrial radiation. They also play a role in atmospheric chemistry.

O<sub>3</sub> – absorbs solar UV radiation; heats the stratosphere; also absorbs some IR

CO<sub>2</sub> – uniformly mixed and so is useful for temperature sounding;  
absorbs IR and so has an important role in atmospheric energy balance

H<sub>2</sub>O – absorbs IR and so determines the radiation budget in the stratosphere;  
involved in cloud formation, precipitation, and energy transport in the troposphere

Although atmospheric constituent measurements began in 1970, routine measurements did not begin until 1978 with the launch of the Nimbus-7 satellite.

### **Nimbus Satellites**

- R&D spacecraft for testing atmospheric remote sounding instruments
- seven Nimbus spacecraft launched between 1964 and 1978
- Nimbus 7 carried a suite of atmospheric instruments:
  - LIMS (Limb Infrared Monitor of the Stratosphere), SAMS (Stratospheric and Mesospheric Sounder), SAM II (Stratospheric Aerosol Measurement II), SBUV/TOMS (Solar Backscatter Ultraviolet/Total Ozone Mapping Spectrometer), ERB (Earth Radiation Budget), SMMR (Scanning Multispectral Microwave Radiometer), THIR (Temperature/Humidity Infrared Radiometer), CZCS (Coastal Zone Color Scanner)

*See table (K&VH 6.1) - satellite measurements of stratospheric gases prior to UARS.*

## Upper Atmosphere Research Satellite (UARS)

Prior to UARS, only a small number of other gases had been measured from satellites: NO, NO<sub>2</sub>, N<sub>2</sub>O, CO, CH<sub>4</sub>, HNO<sub>3</sub>, all of which have a role in atmospheric chemistry and dynamics.

UARS was launched on September 15, 1991 from the Space Shuttle Discovery, to measure the concentrations of many gases involved in stratospheric and mesospheric chemistry. It was the first satellite dedicated to studying stratospheric science.

Ten UARS instruments have provided an extensive data set on upper atmospheric energy inputs, winds, and chemical composition.

### Atmospheric Chemistry and Temperature

- HALOE (Halogen Occultation Experiment) → IR solar occultation using gas correlation cells and broadband channels for O<sub>3</sub>, HCl, HF, CH<sub>4</sub>, H<sub>2</sub>O, NO, NO<sub>2</sub>, aerosols, and T
- ISAMS (Improved Stratospheric and Mesospheric Sounder) → IR limb emission using pressure modulated radiometers for O<sub>3</sub>, CH<sub>4</sub>, CO, H<sub>2</sub>O, NO, NO<sub>2</sub>, N<sub>2</sub>O, HNO<sub>3</sub>, N<sub>2</sub>O<sub>5</sub>, aerosols, and T
- MLS (Microwave Limb Sounder) → microwave limb emission using heterodyne spectroscopy for O<sub>3</sub>, ClO, H<sub>2</sub>O, and T
- CLAES (Cryogenic Limb Array Etalon Spectrometer) → IR limb emission using a Fabry-Perot interferometer for N<sub>2</sub>O, CFC-11, CFC-12, CH<sub>4</sub>, H<sub>2</sub>O, NO, NO<sub>2</sub>, HNO<sub>3</sub>, ClONO<sub>2</sub>, HCl, N<sub>2</sub>O<sub>5</sub>, CO<sub>2</sub>, aerosols, T, and P

*See table (K&VH 6.2) - stratospheric and mesospheric gases measured by UARS*

### Atmospheric Winds

- HRDI (High Resolution Doppler Imager) – wind velocity from 10 to 60 km
- WINDII (Wind Imaging Interferometer) – wind velocity above 80 km

### Energy Inputs

- ACRIM II (Active Cavity Radiometer Irradiance Monitor) – measures the solar constant
- PEM (Particle Environment Monitor) – properties of charged particles
- SUSIM (Solar Ultraviolet Spectral Irradiance Monitor) – solar ultraviolet radiation
- SOLSTICE (Solar-Stellar Irradiance Comparison Experiment) – solar ultraviolet radiation

### Upcoming “Atmospheric Chemistry” Missions

- 1999 – Terra (MOPITT + 4 other instruments)
- 2000 – Meteor 3M (SAGE III)
- 2000 – Odin (SMR, OSIRIS)
- 2001 – Envisat (SCIAMACHY, MIPAS, GOMOS + 5 other instruments)
- 2002 – EOS CHEM (HIRDLS, MLS, TES, and OMI)
- 2002 – SCISAT (ACE, MAESTRO ?)

*See table of Earth Science Missions through 2003 for more comprehensive list.*

Many different techniques and instruments are used to measure atmospheric composition. We will concentrate on measurements of ozone.

## **Measurements of Ozone from Satellites**

Ozone has absorption features in all regions of the EM spectrum and so can be detected using several techniques.

e.g., 21 satellite experiments to measure ozone before 1980; many more since 1980

The three most common techniques use limb or nadir emission (IR or microwave), backscatter ultraviolet (BUV), and solar occultation (UV-visible or IR). A newer technique employs UV-visible limb scattering. *See figure of four viewing geometries.*

### **(1) Ozone Measurements Using Emission**

- usually measure longwave radiation thermally emitted by the atmosphere along the line of sight of the instrument
- infrared (9.6 μm ozone band) or microwave wavelengths
- limb sounding or nadir sounding viewing geometries
- used to retrieve ozone profiles and total columns

General principle:

$$I_{\lambda}(z_1) = I_{\lambda}(0)\tau_{\lambda}(0, z_1) + \int_{\text{surface} \rightarrow \tau_{\lambda}(0, z_1)}^{\text{satellite} \rightarrow \tau_{\lambda}(z_1, z_1)=1} B_{\lambda}(T) d\tau_{\lambda} = I_{\lambda}(0)\tau_{\lambda}(0, z_1) + \int_{\text{surface}}^{\text{satellite}} B_{\lambda}(T) \frac{d\tau_{\lambda}}{dy} dy$$

for no scattering in IR and a satellite at  $z = z_1$ .

In this case,  $T$  is known so  $B(T)$  can be determined. The  $d\tau/dy$  term can be derived and used to calculate the unknown mixing ratio or the optical mass of ozone.

Examples:

Nadir-sounding (see Section 5.1.1)

HIRS (High Resolution Infrared Radiation Sounder)

IRIS (Infrared Interferometer Spectrometer)

Limb-sounding (see Section 5.1.2) – typical vertical resolution is ~3 km

LIMS (Limb Infrared Monitor of the Stratosphere) – 6-channel filter radiometer, 6-15 μm

LRIR (Limb Sounding Infrared Radiometer)

CLAES (Cryogenic Limb Array Etalon Spectrometer)

MLS (Microwave Limb Sounder)

MIPAS (Michelson Interferometer for Passive Atmospheric Sounding) – on ENVISAT

Planned for EOS-CHEM

HiRDLS (High Resolution Dynamics Limb Sounder) – limb scanning

TES (Tropospheric Emission Spectrometer) – limb and nadir viewing

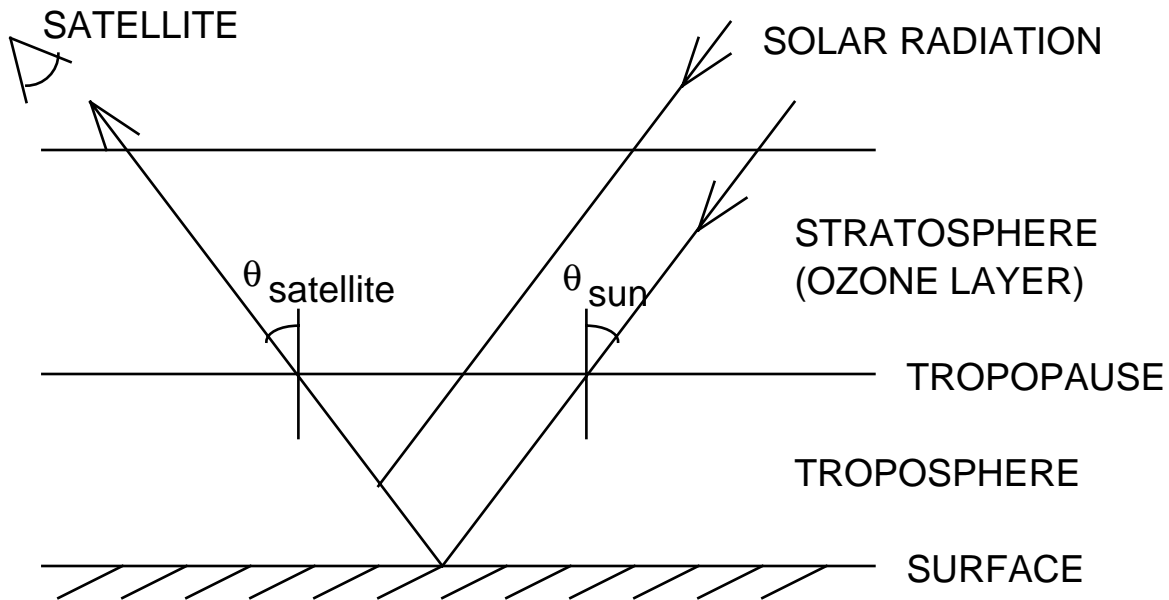
MLS – advanced version, microwave limb viewing

## (2) Ozone Measurements Using UV Backscatter

- probably the best-known method for the retrieval of ozone from satellites
- measure solar UV radiation reflected from the surface and backscattered by the atmosphere or clouds is absorbed by ozone in the Hartley-Huggins bands (< 350 nm)

See figure below. Note:

- most ozone lies in the stratosphere
- most of the backscattered UV radiation comes from the troposphere
- little absorption by ozone occurs in the troposphere
- little scattering occurs in the stratosphere
- radiation reaching the satellite passes through the ozone layer twice



Derivation of the total ozone vertical column:

The satellite measures radiance

$$I(\lambda) = E_{\text{sun}}(\lambda) [\tau_{\text{ozone}}(\lambda)]^x R(\theta_{\text{sun}}, \theta_{\text{satellite}}, R_{\text{surface}}, R_{\text{air}})$$

where

$E_{\text{sun}}(\lambda)$  = solar irradiance at the top of the atmosphere

$[\tau_{\text{ozone}}(\lambda)]^x$  = atmospheric transmission in the ozone band along the slant path, with

$\tau_{\text{ozone}}(\lambda)$  = vertical path transmission

$x = \sec \theta_{\text{sun}} + \sec \theta_{\text{satellite}}$

$R(\theta_{\text{sun}}, \theta_{\text{satellite}}, R_{\text{surface}}, R_{\text{air}})$  = combined surface-troposphere reflectance which depends on zenith angles, reflection from the surface ( $R_{\text{surface}}$ ), and scattering from the air ( $R_{\text{air}}$ )

Recall

$$\tau_{\text{slant}} = \exp\left[-\int \rho k_a ds\right] = \exp\left[-\int \rho k_a \frac{dz}{\cos \theta}\right] = \left\{\exp\left[-\int \rho k_a dz\right]\right\}^{1/\cos \theta} = \{\tau_{\text{vertical}}\}^{\sec \theta}$$

Note: this is a "no emission" form of the RTE, which is applicable at UV-VIS  $\lambda$ , where neither the surface nor the atmosphere emits significant radiation.

Want to solve this equation for the vertical path transmission  $\tau_{\text{ozone}}(\lambda)$ , where

$$\tau_{\text{ozone}}(\lambda) = \exp\left[-\int \rho k_a(\lambda) dz\right] = \exp\left[-\int k_a(\lambda) du\right] = \exp\left[-k_a(\lambda)U\right]$$

with

$k_a(\lambda)$  = mass absorption coefficient

$U$  = total column ozone (molecules/cm<sup>2</sup>)

T and P dependence of  $k_a(\lambda)$  has been ignored (more valid in UV-VIS than in IR)

Thus, if  $\tau_{\text{ozone}}(\lambda)$  can be found, then the total ozone column  $U$  can be calculated. The difficulty is determining the reflectance term  $R$ .

Several satellite instruments measure incoming solar irradiance  $E_{\text{sun}}(\lambda)$  and backscattered radiance  $I(\lambda)$  at two UV wavelengths, one where ozone absorption is strong ( $k_a(\lambda)$  is large) and one where ozone absorption is weak ( $k_a(\lambda)$  is small).

Generate arbitrary quantities (account for logarithmic attenuation)

$$N_1 \equiv -100 \log_{10} \left[ \frac{I(\lambda_1)}{E_{\text{sun}}(\lambda_1)} \right] = -100 \log_{10} [R(\lambda_1) \exp\{-k_a(\lambda_1) U x\}]$$

$$N_2 \equiv -100 \log_{10} \left[ \frac{I(\lambda_2)}{E_{\text{sun}}(\lambda_2)} \right] = -100 \log_{10} [R(\lambda_2) \exp\{-k_a(\lambda_2) U x\}]$$

$$\text{So } N_1 - N_2 = -100 \log_{10} \left[ \frac{R(\lambda_1)}{R(\lambda_2)} \exp\{-[k_a(\lambda_1) - k_a(\lambda_2)] U x\} \right].$$

If  $R$  can be considered constant between the two wavelengths, i.e.,  $R(\lambda_1) = R(\lambda_2)$ , then

$$N_1 - N_2 = -100 \log_{10} [\exp\{-[k_a(\lambda_1) - k_a(\lambda_2)] U x\}]$$

$$\underbrace{N_1 - N_2}_{\text{measure}} = \underbrace{100 \log_{10}(e)}_{\text{constant}} \underbrace{[k_a(\lambda_1) - k_a(\lambda_2)]}_{\text{known}} \underbrace{U}_{\text{retrieve}} \underbrace{x}_{\text{known}}$$

However, the backscattered component,  $R_{\text{air}}$ , has  $\lambda^{-4}$  dependence, so  $R(\lambda_1) \neq R(\lambda_2)$ .

Generally, a third observation at  $\lambda_3$ , outside the ozone band, is used to determine the surface term  $R_{\text{surface}}(\lambda_1) \approx R_{\text{surface}}(\lambda_2)$ , calculate the Rayleigh scattering term  $R_{\text{air}}(\lambda)$ , and thus determine  $R(\lambda_1)$  and  $R(\lambda_2)$ .

Vertical profiles of ozone can also be derived using the “BUV profiling technique”. This relies on the fact that the longer the wavelength of the incoming UV irradiance, the weaker the ozone absorption and so the lower (in z) the penetration of the UV light into the atmosphere. The absorption increases with decreasing wavelength, such that radiation at progressively shorter wavelengths is significantly absorbed at progressively higher altitudes. So the backscattered radiation at specific UV wavelengths can only be scattered from above a particular height. Below this level, all the radiation is absorbed and there is no backscattered radiance. Measurements at certain UV wavelengths are sensitive to specific portions of the ozone vertical profile, and the full profile can be obtained by measuring radiation at a series of wavelengths and using a retrieval algorithm that converts each radiance measurement to an atmospheric quantity.

*See K&VH (pp. 215-216) and Stephens (pp. 294-297) for derivation of ozone profiles from measurements of backscattered UV.*

Examples:

BUV (Backscatter Ultraviolet) instrument

- flew on Nimbus 4, 1970-1977
- two wavelength pairs:  $\lambda_1 = 312.60 \text{ nm}$ ,  $\lambda_2 = 317.63 \text{ nm}$  with  $\lambda_3 = 380 \text{ nm}$   
 $\lambda_1 = 313.29 \text{ nm}$ ,  $\lambda_2 = 339.93 \text{ nm}$

SBUV (Solar Backscatter Ultraviolet) instrument

- flew on Nimbus 7, operated from 1978 to 1990
- two wavelength pairs,  $\lambda_1$ ,  $\lambda_2$ ; and third wavelength  $\lambda_3$

SBUV/2 (Solar Backscatter Ultraviolet 2) instrument

- flown on the NOAA polar orbiter satellites: NOAA-11 (1989 -1994), NOAA-14 (in orbit)
- can measure ozone profiles as well as columns
- takes about seven days to create a global map.

TOMS (Total Ozone Mapping Spectrometer)

- first flew on Nimbus 7, operated from 1978 to 1993
- three subsequent versions: Meteor 3 (1991-1994), ADEOS (1997), Earth Probe (1996-)
- uses three pairs of wavelengths: 313/331, 318/331, 331/340 nm
- measures total ozone columns, creating global maps once a day

GOME (Global Ozone Monitoring Experiment)

- launched on ESA's European Remote Sensing-2 satellite (ERS-2) in 1995
- employs a nadir-viewing BUV technique that measures radiances from 240 to 793 nm
- takes about 2 days to create a global map
- measures ozone columns and profiles, as well as columns of  $\text{NO}_2$ ,  $\text{H}_2\text{O}$ ,  $\text{SO}_2$ , BrO, OClO

### (3) Ozone Measurements Using Occultation

- probably the simplest method for the retrieval of ozone profiles from satellites
- atmospheric extinction at a UV-visible or infrared  $\lambda$  sensitive to ozone absorption is measured from a satellite as the Sun, Moon, or a star rises or sets
- the extinction through the limb of the atmosphere is measured as a function of tangent height, allowing the optical mass to be determined
- vertical resolution is typically 1-2 km, which is better than the UV profiling technique

See figures (Stephens 6.7; and 11.5) – geometry for limb extinction measurements.

Define

$I_\lambda^o$  = intensity at the highest altitude where ozone extinction is zero

$I_\lambda(z_i)$  = intensity measured at the i-th tangent height  $z_i$

The ratio of  $I_\lambda(z_i)$  to  $I_\lambda^o$  is a measure of the transmittance

$$\tau_\lambda(z_i) = \frac{I_\lambda(z_i)}{I_\lambda^o} = \exp\left(-\int_{-\infty}^{\infty} \sigma_{\text{ext},\lambda}(s) ds\right)$$

where

$\sigma_{\text{ext},\lambda}(s)$  = volume extinction coefficient at point  $s$  along the line-of-sight

Typically,  $\sigma_{\text{ext},\lambda}(s) = \sigma_\lambda^{\text{Rayleigh}}(s) + \sigma_\lambda^{\text{ozone}}(s) + \sigma_\lambda^{\text{aerosol}}(s) + \sigma_\lambda^{\text{other gases}}(s)$ .

For a simplified case, ignoring scattering and other sources of extinction:

$$\sigma_{\text{ext},\lambda}(s) = k_a^{\text{ozone}}(\lambda) \rho^{\text{ozone}}(s)$$

$$\text{Thus, } \tau_\lambda(z_i) = \exp\left(-\int_{-\infty}^{\infty} k_a^{\text{ozone}}(\lambda) \rho^{\text{ozone}}(s) ds\right) = \exp\left[-k_a^{\text{ozone}}(\lambda) U^{\text{ozone}}(z_i)\right],$$

ignoring  $T$  and  $p$  dependence of  $k_a^{\text{ozone}}(\lambda)$ .

By measuring  $\tau_\lambda(z_i)$  for a series of tangent heights, a set of columns  $U(z_i)$  can be calculated and then inverted to get the ozone vertical profile.

Note that the same instrument is used to measure the attenuated and unattenuated radiation, so any long-term instrument changes disappear when the ratio is calculated. This is why occultation instruments are often called self-calibrating.

Main disadvantage: Observations are made as the source (usually the Sun) rises or sets relative to the satellite. For a satellite in LEO, this means that there are typically 15 sunset and 15 sunrise measurements per day (maximum = 24 of each). Also, the concentration of some gases changes rapidly during twilight, which can make it difficult to interpret measurements over the long horizontal limb path.

Examples:

The SAGE (Stratospheric Aerosol and Gas Experiment) series

- SAGE flew on AEM 2 (Appl. Explorer Mission), 1979-1981
- SAGE II flew on ERBS (Earth Radiation Budget Satellite), operating since 1984
- SAGE III, scheduled for launch on Russian Meteor-3M in 2000
- all use visible Chappuis band of ozone at 0.6  $\mu\text{m}$ , and other UV-visible channels for the measurement of  $\text{H}_2\text{O}$ ,  $\text{NO}_2$ , and aerosol
- SAGE III will also measure in the near IR, and will have a lunar occultation mode

ATMOS (Atmospheric Trace Molecule Spectroscopy)

- flown on the Space Shuttle four times between 1985 and 1994
- performed solar occultations in the IR using a Fourier transform interferometer
- covered a wide spectral range at high ( $0.015 \text{ cm}^{-1}$ ) resolution, which allowed the retrieval of more than 36 trace gases

HALOE (Halogen Occultation Experiment)

- solar occultation at specific IR wavelengths, flown on UARS

The POAM (Polar Ozone and Aerosol Measurement) series

- POAM II flew on the French Space Agency's SPOT-3, 1993.-1996
- POAM III was launched on SPOT-4 in 1998
- use UV-visible solar occultation to measure profiles of ozone,  $\text{H}_2\text{O}$ ,  $\text{NO}_2$ , aerosols

The ILAS (Improved Limb Atmospheric Spectrometer) series

- solar occultation for high-latitude stratospheric ozone
- ILAS I flew on ADEOS I in 1996, ILAS II scheduled for flight on ADEOS II in 2000

GOMOS (Global Ozone Monitoring by Occultation of Stars)

- scheduled for launch on ENVISAT in 2000
- will perform UV-visible occultation using stars to significantly increase spatial coverage
- disadvantage of the use of the stars is that measurements may not go as low in the atmosphere as solar occultation

ACE (Atmospheric Chemistry Experiment)

- scheduled for launch on Canadian SCISAT in 2002
- IR solar occultation for measurement of >30 trace gases
- may be accompanied by MAESTRO for solar occultation in UV-visible

#### (4) Ozone Measurements Using Limb Scattering

- this a newer technique that combines some of the features of the first three
- has been previously used, but the altitude range was limited to the upper stratosphere and mesosphere – now of interest for the upper troposphere and lower stratosphere
- viewing geometry is similar to that of both limb emission and occultation, which provides good vertical resolution
- measures scattered solar radiation in a manner similar to BUUV, but the light source is in Earth's limb
- provides coverage through the atmosphere, and hence good column measurements

General equation for limb radiance  $I$ , at wavelength  $\lambda$  and tangent height  $z_{\text{tan}}$ , is:

$$\begin{aligned}
 I(\lambda, z_{\text{tan}}) &= E_o(\lambda) \int_{\text{line-of-sight}} \tau_{\text{in}}(\lambda, \infty : z) S(\lambda, z, \theta) \tau_{\text{out}}(\lambda, z : \infty) dz \\
 &= E_o(\lambda) \int_{\infty}^{z_{\text{tan}}} \tau_{\text{in}}(\lambda, \infty : z) S(\lambda, z, \theta) \tau_{\text{out}}(\lambda, z : \infty) dz \\
 &\quad + E_o(\lambda) \int_{z_{\text{tan}}}^{\infty} \tau_{\text{in}}(\lambda, \infty : z) S(\lambda, z, \theta) \tau_{\text{out}}(\lambda, z : \infty) dz
 \end{aligned}$$

where

$E_o(\lambda)$  is the solar irradiance incident on the top of the atmosphere ( $\text{photons cm}^{-2} \text{ s}^{-1} \text{ \AA}^{-1}$ )

$\theta$  is the forward scattering angle

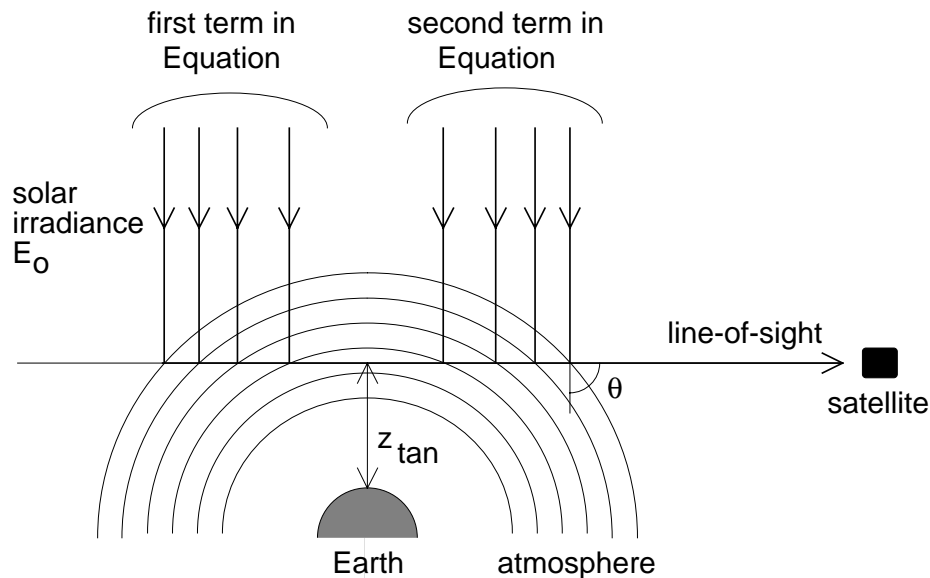
$\tau_{\text{in}}(\lambda, \infty : z)$  is the atmospheric transmission in from the top of the atmosphere to the scattering point at altitude  $z$  along the OSIRIS line-of-sight

$S(\lambda, z, \theta)$  is a scattering term describing the proportion of solar irradiance singly scattered into the instrument line-of-sight

$\tau_{\text{out}}(\lambda, z : \infty)$  is the atmospheric transmission back out from the scattering point at altitude  $z$  along the OSIRIS line-of-sight to the top of the atmosphere

The integral along the line-of-sight is broken down into two terms, corresponding to solar irradiance incident on the atmosphere beyond the tangent point and between the tangent point and the satellite, as illustrated below for a scattering angle of  $90^\circ$ .

Vertical profiles of concentration can be retrieved from UV-visible limb radiance spectra by using a radiative transfer model to simulate the measurements and derive a set of weighting functions. These can then be incorporated into an inversion scheme, such as optimal estimation to derive the trace gas profiles.



Examples:

#### SME (Solar Mesosphere Explorer)

- launched in 1981, carried the first satellite instruments to make such measurements
- mesospheric ozone profiles were retrieved using the Ultraviolet Spectrometer
- stratospheric  $\text{NO}_2$  profiles were retrieved using the Visible Spectrometer
- recorded altitude profiles of scattered sunlight in two spectral channels (265/296.4 nm and 439/442 nm), and a single scattering RT model was used for inversion of the data

MSX satellite – launched in April 1996 with a 5-year lifetime, carries a suite of UV-visible sensors (UVISI) to observe the limb from 110 to 900 nm

#### SOLSE

- flown on the Space Shuttle flight in 1997
- imaged the limb onto a charge-coupled-device detector array through a spectrometer to simultaneously obtain spectra from 260 to 350 nm at a range of tangent heights
- has given good ozone profiles with high vertical resolution down to the tropopause

#### OSIRIS (Optical Spectrograph and Infrared Imaging System)

- scheduled for launch on Odin in 2000 (Canadian instrument)
- will scan the limb from ~10 km to as high as 120 km, recording spectra of scattered from 280 to 800 nm for the retrieval of vertical profiles of ozone,  $\text{NO}_2$ ,  $\text{OCIO}$ ,  $\text{BrO}$ ,  $\text{NO}_3$ ,  $\text{O}_2$ , and aerosols

#### SCIAMACHY (Scanning Imaging Absorption SpectroMeter for Atmospheric CHartography)

- scheduled for launch on ENVISAT-1 in 2000
- will provide global measurements of various trace gases in the troposphere and stratosphere by measuring transmitted, backscattered, and reflected radiation from the atmosphere between 240 and 2400 nm
- uses both nadir and limb scanning geometry

**Advantages and disadvantages of these four measurement techniques:**

TECHNIQUE	ADVANTAGES	DISADVANTAGES
Emission	<ul style="list-style-type: none"><li>• doesn't require sunlight</li><li>• long time series</li><li>• simple retrieval technique</li><li>• provide global maps twice a day (good spatial coverage)</li></ul>	<ul style="list-style-type: none"><li>• slightly less accurate than backscatter UV</li><li>• long horizontal path for limb obs.</li></ul>
Backscatter UV	<ul style="list-style-type: none"><li>• accurate</li><li>• long time series</li><li>• good horizontal resolution due to nadir viewing</li></ul>	<ul style="list-style-type: none"><li>• requires sunlight, so can't be used at night or over winter poles</li><li>• poor vertical resolution below the ozone peak (~30 km) due to the effects of multiple scattering and reduced sensitivity to the profile shape</li></ul>
Occultation	<ul style="list-style-type: none"><li>• simple equipment</li><li>• simple retrieval technique</li><li>• good vertical resolution</li><li>• self-calibrating</li></ul>	<ul style="list-style-type: none"><li>• can only be made at satellite sunrise and sunset, which limits number and location of meas.</li><li>• long horizontal path</li></ul>
Limb Scattering	<ul style="list-style-type: none"><li>• excellent spatial coverage</li><li>• good vertical resolution</li><li>• data can be taken nearly continuously</li></ul>	<ul style="list-style-type: none"><li>• complex viewing geometry</li><li>• poor horizontal resolution</li></ul>

## Ozone Monitoring Satellite Missions

*Refer to figure of Satellite Ozone Monitoring (from “Stratospheric Ozone, An Electronic Textbook” by NASA's Goddard Space Flight Center Atmospheric Chemistry and Dynamics Branch).*

Major ozone-related missions and instruments (previous, current, and planned)

- Nimbus 7 – LIMS, SBUV, TOMS
- NOAA series – SBUV/2
- four TOMS missions
- three SAGE missions
- UARS – HALOE, ISAMS, MLS, CLAES
- ERS-2 – GOME
- Odin – OSIRIS, SMR
- ENVISAT – SCIAMACHY, MIPAS, GOMOS
- SCISAT – ACE, MAESTRO ?
- EOS-CHEM – HIRDLS, MLS, TES, OMI
- METOP (Meteorological Operational) satellites – new GOME
- ADEOS-II (Advanced Earth Observing Satellite-II) – ILAS II
- NPOESS (National Polar-Orbiting Operational Environmental Satellite System)  
→ developing a replacement for the NOAA-14 SBUV/2 instrument to measure the ozone profile with better vertical resolution and altitude coverage
- Space Shuttle  
→ SSBUV – eight flights  
→ CRISTA-SPAS (Cryogenic Infrared Spectrometers and Telescopes for the Atmosphere-Shuttle Pallet Satellite) – German instrument launched in 1997  
→ MAHRSI (Middle Atmosphere High Resolution Spectrographic Investigation)  
→ SOLSE/LORE – 1997 flight

## **5.3 Measurements of Clouds, Aerosols, and Precipitation**

### ***References***

- *Kidder and Vonder Haar: chapter 5, pp. 145-154; parts of chapters 8, 9*
- *Stephens: chapter 6, pp. 261-271; chapter 7, pp. 347-355, 368-385; parts of chapter 8*
- *Houghton, Taylor, and Rodgers: chapter 3; chapter 11*
- *Liou: chapter 7, pp. 285-289*

First, need to define clouds and aerosols. Why are they important?  
Recall our earlier definitions:

### **Clouds**

- consist of water drops and ice crystals of radius  $\sim 10 \mu\text{m}$
- are classified on the basis of size:  

<u>cloud drops</u>	$r = 10 \mu\text{m}$
<u>drizzle</u>	$r = 100 \mu\text{m}$
<u>rain drops</u>	$r = 1000 \mu\text{m}$ (1 mm)

### **Aerosols**

- are particles suspended in a gas  
e.g., haze and dust particles, volcanic debris, pollen, sea salt, sulphates and nitrates
- are produced by natural and anthropogenic sources
- are classified on the basis of size:  

<u>Aitken</u> particles	$r < 0.1 \mu\text{m}$
<u>large</u> particles	$0.1 \leq r \leq 1 \mu\text{m}$
<u>giant</u> particles	$r > 1 \mu\text{m}$

*See figure (Stephens 1.10) – names of atmospheric particles.*

Clouds cover  $\sim 50\%$  of the Earth. Aerosols are always present in the atmosphere.

### **Clouds and aerosols:**

- influence Earth's radiation budget
- influence climate
- interfere with radiometric observations of the atmosphere and surface
- are linked to daily weather (clouds)

### **5.3.1 Observations of Clouds**

#### **(1) Imaging of Clouds**

This is a straightforward technique that can be used to

- detect and identify clouds
- determine the physical mechanisms that produced them

The fractional cloud cover as a function of space and time is a basic meteorological parameter, and is used in weather forecasting. The appearance of cloud patterns can usually be related to fronts, storms, depressions, hurricanes, etc..

Spectral bands used by meteorological satellites:

(i) Visible imagery

- 0.4 to 0.7  $\mu\text{m}$
- high spatial resolution
- easy to recognize land, ocean, and cloud
- limited to sunlit conditions

(ii) Infrared imagery

- usually between 1 and 30  $\mu\text{m}$
- most commonly used in the 10-12.5  $\mu\text{m}$
- land, ocean, and clouds are easily recognizable
- provides nighttime images
- can be related to atmospheric temperature and surface temperature

(iii) Water vapour imagery

- observations are made in water vapour absorption bands, usually at 6.7  $\mu\text{m}$
- radiation comes from 300-600 mbar (mid-troposphere)
- used to approximate relative humidity in this region, and to identify rising and sinking air

(iv) Microwave imagery

- different wavelengths are sensitive to different features
- e.g., 19 GHz – window region, sees surface in absence of cloud  
22 GHz – sensitive to water vapour  
37 GHz – sensitive to clouds, rain  
85 GHz – sensitive to ice clouds, snow

Often the information from several spectral bands is combined.

*See figures (K&VH 5.5, 5.6) – visible and infrared cloud images.*

Figure 5.5

Low level cloud is not seen in the IR image because it is at a temperature  $\approx T_{\text{surface}}$ . However, it is seen in the visible image, because it is brighter than the surface.

Figure 5.6

High level (cirrus) cloud is not seen in the visible image because it is transparent to these wavelengths. However, it is seen in the IR image because it is cold and opaque to IR radiation from the warm surface below.

Thick cloud is seen in both the visible and IR. Low cloud is seen in the visible, but not in the IR. High cloud is seen in the IR, not in the visible.

A bispectral cloud classification scheme:

		VISIBLE	
		DARK	BRIGHT
INFRARED	COLD	thin high cirrus	deep convective clouds
	WARM	no clouds	low clouds

Infrared - greater radiance, darker pixel so that warmer ground is darker than cool clouds.  
Visible - greater radiance, brighter pixels.

Clouds can be highly informative features on satellite images, with both their extent and character providing information.

*See K&VH (p. 165, 269) for more details, and techniques for determining cloud cover.*

## (2) Sounding of Clouds

In addition to mapping clouds using images, further information about clouds is needed:

- to eliminate the effects of clouds from temperature sounding experiments
- to interpret radiation budget measurements
- to parameterize clouds for numerical modelling
- to locate areas of precipitation and estimate the level of precipitation

For these purposes, useful cloud properties include:

- cloud coverage/amount (from imagers)
- cloud top height (or pressure)
- emittance
- phase (ice or water)
- drop size distribution
- cloud top temperature
- reflectance
- optical depth
- liquid water content

Sounders can be used to determine some of these properties and also to remove cloud contamination in order to obtain clear column radiances.

Assuming that a sounder operates at a  $\lambda$  at which clouds have negligible reflectance, then the measured radiance is

$$I(\lambda) = (1 - N)I_{\text{clear}}(\lambda) + N\epsilon I_{\text{cloud}}(\lambda) + N(1 - \epsilon)I_{\text{clear}}(\lambda)$$

where

$I_{\text{clear}}(\lambda)$  = radiance if no cloud were present

$I_{\text{cloud}}(\lambda)$  = radiance emitted by the cloud if it were a blackbody

$N$  = fractional cloud amount

$\epsilon$  = cloud emittance

$1 - \epsilon$  = cloud transmittance

first term = radiation from clear area  
 second term = radiation emitted by the cloud  
 third term = radiation transmitted through the cloud

Combining the first and third terms:

$$I(\lambda) = (1 - N')I_{\text{clear}}(\lambda) + N'I_{\text{cloud}}(\lambda)$$

where

$N' \equiv N\epsilon = \text{effective cloud amount}$ .

This equation is used to determine clear-column radiances, the effective cloud amount, and the cloud-top pressure.

Procedure:

A radiometer measures  $I_1(\lambda)$  and  $I_2(\lambda)$  at two adjacent scan spots for which  $I_{\text{clear}}(\lambda)$ ,  $I_{\text{cloud}}(\lambda)$ , and  $\epsilon$  are equal, i.e.,

- the clouds have basically the same height and composition at both spots
- the land surface and clear atmosphere are the same.

Only the cloud amounts  $N_1'$  and  $N_2'$  differ.

Thus have

$$\begin{aligned} I_1(\lambda) &= (1 - N_1')I_{\text{clear}}(\lambda) + N_1'I_{\text{cloud}}(\lambda) \\ I_2(\lambda) &= (1 - N_2')I_{\text{clear}}(\lambda) + N_2'I_{\text{cloud}}(\lambda) \end{aligned}$$

Eliminate  $I_{\text{cloud}}(\lambda)$  to get  $I_{\text{clear}}(\lambda) = \frac{I_1(\lambda) - N^*I_2(\lambda)}{1 - N^*}$  where  $N^* \equiv \frac{N_1'}{N_2'}$ .

Thus, measurement of  $I_1(\lambda)$ ,  $I_2(\lambda)$ , and  $N^*$  will yield  $I_{\text{clear}}(\lambda)$ .

*See K&VH (p. 261-264) for methods of retrieving  $N^*$ .*

Cloud amount and cloud-top pressure can be retrieved from sounder data using either:

- radiance residual methods - applied after a sounding has been used to obtain clear-column radiances and profiles of T and H<sub>2</sub>O (compare  $I(\lambda)$  with calculated I for set of cloud-top pressures)
- radiance ratio methods - require data from two sounding channels so that the radiances at two wavelengths can be compared

These methods give reasonable results for cloud amount and cloud-top pressure in the mid to upper troposphere with moderate to large cloud amounts. Retrievals are poor for the lower troposphere and smaller cloud amounts.

### (3) Microwave Radiometry and Clouds

Microwave observations can be used to measure the liquid water content (LWC) of clouds.

Water vapour absorption has a peak at 22 GHz.

Liquid water absorption increases with  $\nu$  in the microwave.

$\therefore$  Measuring radiances at 22 GHz and at 31 GHz (window) allows both the column water vapour and the column liquid water content to be retrieved.

Recall the Rayleigh-Jeans Approximation:  $B_\lambda(T) = \frac{c_1}{c_2} \frac{T}{\lambda^4}$

This can be combined with Schwarzschild's Equation to get

$$T_B \approx T_o \left\{ 1 - [1 - \epsilon_o(\mu)] \tau_o^{2/\mu} \right\}$$

where

$T_B$  = brightness temperature

$T_o$  = surface temperature

$\epsilon_o$  = surface emittance

$\tau_o$  = vertical transmission from surface to satellite

$T_o$  and  $\epsilon_o$  contain information on the surface properties.

$\tau_o$  contains information on the atmospheric properties.

Define  $U_L$  = column liquid water content  
 $U_V$  = column water vapour (= precipitable water)

$$\text{Then } \tau_o^{2/\mu} = \exp \left[ -\frac{2}{\mu} (k_L U_L + k_V U_V) \right] \approx \frac{T_o - T_B}{[1 - \epsilon_o(\mu)] T_o}$$

$$\text{so } k_L U_L + k_V U_V \approx -\frac{\mu}{2} \ln \left[ \left( \frac{T_o - T_B}{[1 - \epsilon_o(\mu)] T_o} \right) \right].$$

This equation can be applied at two microwave frequencies (e.g., 22 and 31 GHz), with  $T_o$  and  $\epsilon_o$  constant, to solve for  $U_L$  and  $U_V$ .

Note: Independent measurements of liquid water for comparison with satellite measurements are essentially nonexistent, so the accuracy of the satellite measurements cannot be determined!

### 5.3.2 Observations of Aerosols

Remote sounding techniques for aerosols differ for stratospheric and tropospheric aerosols. We consider each separately.

#### **Stratospheric Aerosols**

→ have low number densities: 1 to 10 particles / cm<sup>3</sup>

Therefore, limb scanning solar occultation is the most commonly used technique for remote sounding of stratospheric aerosols.

- provides a long pathlength which increases the extinction along the line-of-sight
- self-calibrating – so variations in solar output and instrumental gain are removed by ratioing the attenuated radiance to the unattenuated solar radiance

e.g. SAM (Stratospheric Aerosol Measurement) – 1970s

SAGE – four channels:

0.385 μm, 0.45 μm (both sensitive to aerosol and NO<sub>2</sub>)

0.6 μm (ozone and aerosol)

1.0 μm (aerosol only)

SAGE II – seven channels: 0.385, 0.448, 0.453, 0.525, 0.6, 0.936 (H<sub>2</sub>O), 1.02 μm

Recall the equation for atmospheric transmittance for a solar occultation measurement:

$$\tau_{\lambda}(z_i) = \frac{I_{\lambda}(z_i)}{I_{\lambda}^o} = \exp\left(-\int_{-\infty}^{\infty} \sigma_{\text{ext},\lambda}(s) ds\right)$$

so limb OD is 
$$\delta_{\lambda}(z_i) = \int_{-\infty}^{\infty} \sigma_{\text{ext},\lambda}(s) ds = -\ln[\tau_{\lambda}(z_i)]$$

where

$I_{\lambda}^o$  = intensity at the highest altitude where extinction is zero

$I_{\lambda}(z_i)$  = intensity measured at the i-th tangent height  $z_i$

$\sigma_{\text{ext},\lambda}(s)$  = volume extinction coefficient at point  $s$  along the line-of-sight

with

$$\begin{aligned} \sigma_{\text{ext},\lambda} &= \sigma_{\lambda}^{\text{Rayleigh}} + \sigma_{\lambda}^{\text{aerosol}} + \sigma_{\lambda}^{\text{gases}} \\ &= \sigma_{\lambda}^{\text{Rayleigh}} + \sigma_{\lambda}^{\text{aerosol}} + \sigma_{\lambda}^{\text{ozone}} + \sigma_{\lambda}^{\text{NO}_2} \quad (\text{typically, for SAGE measurements}) \end{aligned}$$

See figure (Stephens 6.8) – volume extinction coefficient as function of wavelength.

Two approaches to the retrieval of  $\sigma_{\lambda}^{\text{aerosol}}(z)$  (and  $\sigma_{\lambda}^{\text{Rayleigh}}$ ,  $\sigma_{\lambda}^{\text{ozone}}$ ,  $\sigma_{\lambda}^{\text{NO}_2}$ ) from a set of occultation measurements at several wavelengths and a range of tangent heights:

(1) SAGE data processing

- generate profiles of the limb optical depth  $\delta_{\lambda}(z_i)$  for each channel
- subtract the estimated Rayleigh contribution along each limb path for each channel
- separate the aerosol, ozone, and NO<sub>2</sub> contributions to the optical depths
- divide the atmosphere into N homogeneous layers to reduce the integral equation for OD into a system of linear equations

$$\delta_{\lambda}^{\text{aerosol}}(z_i) = \sum_{j=1}^N \sigma_{\lambda}^{\text{aerosol}}(z_j) \Delta s(z_i, z_j)$$

where  $\Delta s(z_i, z_j)$  is the path length of the Sun's ray in the j-th layer with the tangent height in the i-th layer (similar equations for ozone and NO<sub>2</sub>)

- invert this system of equations with a version of Chahine's retrieval method to convert the aerosol, ozone, and NO<sub>2</sub> optical depths into extinction profiles

(2) It is possible to show that

$$\sigma_{\text{ext},\lambda}(z_i) = \frac{1}{\pi} \int_{z_i}^{\infty} \frac{d\tau_{\lambda}}{dz} \frac{1}{\sqrt{(z + R_E)^2 - (z_i + R_E)^2}} dz$$

peaks at  $z = z_i$  so most info is from tangent point

and apply this equation to derive extinction profiles for each of the  $\sigma_{\lambda}$  terms.

Final product: vertical profiles of the aerosol extinction coefficient,  $\sigma_{\lambda}^{\text{aerosol}}(z)$ , at ~10% accuracy from the tropopause to ~25 km.

SAGE II data products also include:

- aerosol optical depth at 385, 453, 525 and 1020 nm integrated above the tropopause
- aerosol surface area density

*See figure (K&VH 8.15) – typical vertical profiles of aerosol extinction at SAGE II wavelengths.*

Such measurements have been used:

- to monitor polar stratospheric clouds which play a role in polar ozone depletion  
*See figures (Stephens 6.9, 6.10) – contour plots of average extinction ratio (6.9) and the volume extinction coefficient as function of wavelength (6.10).*

- to detect and map the movement of volcanic aerosol clouds

*See figures of “SAGE aerosol optical depth before and after Mount Pinatubo” and “long-term aerosol optical depth”.*

- to monitor global background aerosol extinction

*See figures of “aerosol surface density” and “aerosol surface area”.*

## Tropospheric Aerosols

→ have high number densities: ~1000 times greater than those of stratospheric aerosols

Remote sounding of tropospheric aerosols is also based on measurement of scattered radiation (aerosol extinction) but with the Earth's surface as the background, i.e., nadir observations.

However, retrieval of aerosol properties from space-based measurements of reflected sunlight is difficult because of:

- the relatively small effect of aerosol on reflected sunlight, which therefore requires accurate measurement of intensities
- the variability of the surface features and properties
- the influence of aerosol microphysics on the reflection of sunlight

The radiance measured from a nadir-viewing satellite instrument in the UV-visible-near IR (i.e. no emission) can be written as:

$$I(\lambda) = I_o(\lambda)\tau_o(\lambda) + I_{\text{Rayleigh}}(\lambda) + I_{\text{aerosol}}(\lambda)$$

where

$I_o(\lambda)$  = radiance leaving the surface

$\tau_o(\lambda)$  = transmittance from the surface to the satellite

$I_{\text{Rayleigh}}(\lambda)$  = radiance term due to Rayleigh scattering by air molecules

$I_{\text{aerosol}}(\lambda)$  = radiance term due to scattering of sunlight by aerosols

At red and near infrared wavelengths,  $I_o(\lambda) \approx 0$  over the oceans, except in areas of:

(1) sun glint (reflection from the rough ocean surface)

(2) suspended particles (e.g., plankton)

where the aerosol signal is lost in the bright background signal.

If  $I_o(\lambda) \approx 0$  and  $I_{\text{Rayleigh}}(\lambda)$  can be modelled and corrected for, then it can be shown that the solution of the Radiative Transfer Equation is

$$I_{\text{aerosol}} \cong \frac{\tilde{\omega}_o}{4\pi} E_{\text{sun}} p(\Psi_{\text{sun}}) \frac{1}{\mu} \int_{\text{surface}}^{\text{satellite}} \sigma_{\text{aerosol}} dz = \frac{\tilde{\omega}_o}{4\pi} E_{\text{sun}} p(\Psi_{\text{sun}}) \frac{1}{\mu} \delta_{\text{aerosol}}$$

where

$E_{\text{sun}}$  = solar irradiance (can be measured or calculated from the time of year, solar spectrum, and spectral response of the instrument)

$\mu$  =  $\cos \theta$

$\Psi_{\text{sun}}$  = scattering angle between the Sun and the satellite

$\tilde{\omega}_o$  = single scatter albedo =  $\sigma_s / \sigma_{\text{ext}}$

$p(\Psi_{\text{sun}})$  = scattering phase function

$\delta_{\text{aerosol}}$  = vertical aerosol optical depth

Thus: 
$$\delta_{\text{aerosol}} = \frac{4\pi\mu}{\tilde{\omega}_o p(\Psi_{\text{sun}})} \frac{I_{\text{aerosol}}}{E_{\text{sun}}}$$

$E_{\text{sun}}$ ,  $\mu$ , and  $\Psi_{\text{sun}}$  can all be determined, however,  $\tilde{\omega}_o$  and  $p(\Psi_{\text{sun}})$  depend on the index of refraction and the size distribution of the aerosols.

Therefore some knowledge of the microphysical properties of the aerosol is needed before the aerosol optical depth,  $\delta_{\text{aerosol}}$ , can be retrieved. It can sometimes be assumed that  $\tilde{\omega}_o = 1$  (i.e., the aerosol particles are nonabsorbing). Some assumption or model for  $p(\Psi_{\text{sun}})$  and its dependence on particle size is usually required.

Example: One approach is to take the ratio of the intensities at two wavelengths,

$$S_{12} = \frac{I_1}{I_2} \cong \frac{[\tilde{\omega}_o p(\Psi_{\text{sun}}) \delta_{\text{aerosol}}]_1}{[\tilde{\omega}_o p(\Psi_{\text{sun}}) \delta_{\text{aerosol}}]_2}$$

and use it to parameterize the scattering phase function. This has been done with channels 1 (red) and 2 (near IR) of AVHRR (Advanced Very High Resolution Radiometer). Changes in the aerosol size distribution cause changes in the optical depths and the phase functions and hence result in spectral variations in the measured intensities. It is possible to relate  $S_{12}$  to the aerosol size distribution and then derive a relation between  $p(\Psi_{\text{sun}})$  and  $S_{12}$ .

Studies of tropospheric aerosols have included measurements of the aerosol optical depth of (1) marine aerosols, and (2) Saharan dust. Accuracies range from 10% to 50%.

*See figure (K&VH 8.16) – aerosol optical depths.*

### Active (LIDAR) Remote Sounding of Aerosols

Space-based active remote sounding of the atmosphere has not been widely used to date, but it is a powerful technique which is receiving increasing attention. Lidar instruments have been flown on aircraft and the LITE (Lidar In-space Technology Experiment) mission, the first lidar designed for atmospheric studies to fly in Earth orbit, was flown on the Space Shuttle in September 1994.

<b>LITE Science Objectives</b> (measurements made at 355, 532, and 1064 nm)			
<b>Tropospheric Aerosols</b>	<b>Stratospheric Aerosols</b>	<b>Clouds</b>	<b>Surface Reflectance</b>
aerosol scattering ratio and wavelength dependence	aerosol scattering ratio and wavelength dependence	vertical distribution, multilayer structure	albedo
PBL height and structure	averaged integrated backscatter	fractional cloud cover	multiangle backscatter ( $\pm 30^\circ$ )
PBL optical depth	stratospheric density and temperature	optical depth	

Lidar is ideally suited for detecting and profiling aerosol layers and tenuous clouds, even at night or over inhomogeneous terrain.

Recall the five types of lidar:

- backscatter lidar
- differential absorption lidar (DIAL)
- Doppler lidar
- fluorescence lidar
- Raman lidar

We will look at the first two, as they are the most commonly used for atmospheric applications.

### (1) Backscatter Lidar

- generally consists of a non-tunable high-power pulsed laser and an incoherent detection system (i.e., intensity of the received signal is measured, but not its phase)
- a narrow beam is transmitted into the atmosphere and backscattered by the atmosphere to a receiver telescope and detector
- the nature of the backscattering is determined by the properties of the volume of the atmosphere that contains the Rayleigh and aerosol (Mie) scatterers
- the combination of the short laser pulse ( $\sim 10^{-8}$  sec) and the small beam divergence ( $\sim 10^{-3}$  to  $10^{-4}$  radians) results in compact lidar volumes of a few cubic metres at ranges of tens of km
- the primary properties measured are the intensity and polarization of the beam, and these are used to retrieve

The backscattered radiation received by a lidar detector is given by the general lidar equation:

$$P_r(\lambda, R) = P_t(\lambda)C(\lambda) \frac{\Delta R}{R^2} \frac{\beta(\lambda)}{4\pi} \exp\left[-2 \int_0^R \sigma_{\text{ext}}(\lambda, r) dr\right]$$

where

$P_r(\lambda, R)$  = power received by the system after backscattering from range R

$P_t(\lambda)$  = power transmitted (sometimes this is folded into  $C(\lambda)$ )

$C(\lambda)$  = lidar calibration constant, which includes losses in the transmitting and receiving optics, the effective receiver aperture, and other instrument factors

$\frac{\beta(\lambda)}{4\pi}$  = backscattering coefficient (in units of  $\text{length}^{-1} \text{ster}^{-1}$ ) which depends on the properties (size, shape, composition, density, etc.) of the scattering particles

$\Delta R$  = lidar range resolution =  $h/2$ , where h is the length of the emitted pulse

$\sigma_{\text{ext}}(\lambda, r)$  = volume extinction coefficient

*See figure (Stephens 8.15) – backscatter profiles. Illustrates how different sources of backscatter contribute to the measured profiles and how the backscattering decays ~exponentially with range as the lidar pulse is attenuated by the clouds.*

Most of the information about atmospheric properties derived from backscatter lidar measurements is in the extinction and backscatter coefficients  $\sigma_{\text{ext}}(\lambda, r)$  and  $\beta(\lambda)$ .

The retrieval of aerosol properties from the lidar equation thus requires the inversion of the lidar equation. One approach to this begins with the definition of the signal variable

$$S(R) = \ln[R^2 P_r(R)]$$

(dropping the wavelength dependence for clarity).

By defining a reference value  $S_o = S(R_o)$  at reference range  $R_o$ , the lidar equation can be rewritten as

$$S - S_o = \ln\left(\frac{\beta}{\beta_o}\right) - 2 \int_{R_o}^R \sigma_{\text{ext}} dr$$

(also dropping the range dependence for clarity).

In differential form, this becomes 
$$\frac{dS}{dR} = \frac{1}{\beta} \frac{d\beta}{dR} - 2\sigma_{\text{ext}}$$

In order to solve this equation, a relationship (the “backscattering-to-extinction ratio”) between  $\beta$  and  $\sigma_{\text{ext}}$  is needed.

Special case: 
$$\frac{d\beta}{dR} = 0$$

This assumes that the scattering particles are homogeneously distributed along the lidar line-of-sight. In this case, the extinction coefficient  $\sigma_{\text{ext}}$  can simply be derived from the slope of  $S$  vs. range  $R$ . This is called the slope method of inversion.

More general case (*Carswell, Can. J. Phys.*, **61**, 378, 1983):

More often, the scatterers are inhomogeneously distributed, and so an a priori relationship between  $\beta$  and  $\sigma_{\text{ext}}$  is assumed, usually of the form  $\beta = b\sigma_{\text{ext}}^n$ . Substituting this into the differential equation derived above gives

$$\frac{dS}{dR} = \frac{n}{\sigma_{\text{ext}}} \frac{d\sigma_{\text{ext}}}{dR} - 2\sigma_{\text{ext}}$$

for which the general solution at range  $R$  is 
$$\sigma_{\text{ext}} = \frac{\exp[(S - S_o)/n]}{\frac{1}{\sigma_{\text{ext},o}} - \frac{2}{n} \int_{R_o}^R \exp[(S - S_o)/n] dr}$$

where

$\sigma_{\text{ext},o}$  = extinction coefficient at the reference range  $R_o$ .

There are two problems with this inversion: (i) the validity of the assumed relationship between  $\beta$  and  $\sigma_{\text{ext}}$ , and (ii) the instability of the solution relative to  $\sigma_{\text{ext},o}$ . The signal decreases as  $R$  increases  $> R_o$ , and so the above solution becomes the ratio of two numbers which are both decreasing as the range increases.

Alternative solution (the Klett method):

The reference extinction coefficient is defined at an end range  $R_m$ , so that the solution is obtained for  $R \leq R_m$  instead of for  $R \geq R_o$ , and becomes

$$\sigma_{\text{ext}} = \frac{\exp[(S - S_m) / n]}{\frac{1}{\sigma_{\text{ext},m}} - \frac{2}{n} \int_R^{R_m} \exp[(S - S_m) / n] dr}$$

This small change removes the instability as the solution is the ratio of two numbers which are both increasing as the range increases. This approach is one of the most commonly employed for the retrieval of aerosol properties using ground-based backscatter lidars.

*See figure (Stephens 8.16) – vertical profiles of lidar backscatter and long-term variation.*

Backscatter lidars have also been flown on aircraft and on the Space Shuttle (LITE).

*See figures – LITE aerosol measurements.*

*See Stephens, Section 8.4.3 for discussion of high spectral resolution backscatter lidar which can be used to distinguish between Rayleigh and aerosol scattering and thereby eliminate the need for assumptions about the backscattering-to-extinction ratio.*

## (2) Differential Absorption Lidar (DIAL)

- consists of similar components to a backscatter lidar, but transmits pulses at two adjacent wavelengths which are characterized by different gas absorption strengths (strong and weak – on and off an absorption feature)
- the difference in the backscattered signal can be related to the absorption of the gas
- the primary property measured is the extinction of the beam, which is used to retrieve trace gas concentrations

*Additional reference: S. Svanberg, “Differential Absorption Lidar (DIAL)”, Chapter 3 of Air Monitoring by Spectroscopic Techniques, M.W. Sigrist, ed., New York: John Wiley & Sons Inc., 1994.*

The volume extinction coefficient can be considered as:

$$\sigma_{\text{ext}} = \sigma_{\text{aerosol}} + \sigma_{\text{abs}} = \sigma_{\text{aerosol}} + \rho k_{\text{abs}}$$

where the extinction due to aerosol scattering and due to gaseous absorption have been separated, and  $\rho$  is the number density of the absorbing gas.

The concentration of the gas could be derived directly from the lidar equation using some inversion scheme such as Klett's. However, it is much simpler to apply the DIAL approach, as it does not require knowledge of  $\beta$ ,  $\sigma_{\text{aerosol}}$ , and  $\sigma_{\text{abs}}$ .

Measurements are made at two wavelengths,  $\lambda_1$  and  $\lambda_2$ , that are close enough that  $\beta(\lambda_1) \cong \beta(\lambda_2)$  and  $\sigma_{\text{aerosol}}(\lambda_1) \cong \sigma_{\text{aerosol}}(\lambda_2)$ . Then taking the ratio of the lidar equation applied at each of these wavelengths yields

$$\ln \left[ \frac{P_1(R)}{P_2(R)} \right] \cong -2 \int_0^R \rho [k_1 - k_2] dr$$

where  $P_1$  and  $P_2$  are the backscattered signals normalized to the transmitted signals at each wavelength, i.e.,  $P_1 = P_r(\lambda_1) / P_t(\lambda_1)$  and  $P_2 = P_r(\lambda_2) / P_t(\lambda_2)$ , while  $k_1 = k_{\text{abs}}(\lambda_1)$  and  $k_2 = k_{\text{abs}}(\lambda_2)$ .

This equation can be solved for the number density  $\bar{\rho}(R)$ , averaged over the lidar volume that extends from  $R$  to  $R + \Delta R$ :

$$\bar{\rho}(R) = \frac{\ln \left[ \frac{P_1(R + \Delta R)}{P_2(R + \Delta R)} \right] - \ln \left[ \frac{P_1(R)}{P_2(R)} \right]}{2(k_1 - k_2)\Delta R}$$

From this equation, it can be seen that the range interval  $\Delta R$  must be sufficiently large to provide a measurable average number density.

*See figure (Svanberg 3.16) – principle of differential absorption lidar.*

Ground-based and airborne DIAL systems have been used to measure water vapour, ozone,  $\text{NO}_2$ ,  $\text{NO}$ ,  $\text{SO}_2$ , and Hg.

*See figures (Browell 5 and 6) – airborne DIAL ozone profiles.*

## Future Lidar Missions

- PICASSO-CENA (Pathfinder Instruments For Cloud And Aerosol Spaceborne Observations-Climatologie Etendue des Nuages et des Aerosols)
  - will fly a polarization-sensitive lidar (532, 1064 nm) to get high resolution vertical profiles of aerosols and clouds
  - will also carry three passive instruments in formation with EOS PM to obtain coincident observations of radiative fluxes and the atmospheric state
  - launch planned for 2003
- ORACLE (tentative)
  - DIAL system intended to operate at 308, 320, 524, and 747 nm for the measurement of ozone profiles from the PBL to 50 km at  $\leq 10\%$ , aerosols, PSCs

### **5.3.3 Observations of Precipitation**

#### ***References***

- *Kidder and Vonder Haar: chapter 9*
- *Stephens: chapter 8*
- *Kummerow et al., J. Atmos. Oceanic Technology, 15, 809-817, 1998.*

Precipitation is a key component of the Earth's hydrological cycle:

- the atmosphere gets 75% of its heat energy from release of latent heat by precipitation
- about two-thirds of this precipitation falls in the tropics
- differences in large-scale rainfall patterns and their associated energy release in the Tropics, in turn, affect the entire global circulation, e.g., El Nino
- precipitation is highly variable and the "average" rainfall is rarely observed – instead periods of drought are often followed by periods of torrential rain and flooding
- rain and its latent heating are key to the initialization of global weather and climate models, all of which inadequately predict precipitation and soil moisture (and differ widely in the amount of global warming resulting from doubling of CO<sub>2</sub>)

Quantitative estimates of tropical precipitation vary by as much as 100%, depending upon the estimates. These differences are due to both the lack of good direct measurements of rainfall, as well as the highly variable nature of the parameters both spatially and temporally.

Precipitation can be measured locally at ground level using

- rain gauges – highly accurate but only sample volumes of ~0.1 m<sup>2</sup>
- radar techniques – cover larger volumes but typically have an accuracy of a factor-of-2

We currently need better observations of global precipitation and to incorporate more realistic cloud processes into atmospheric models.

With 75% of the tropics covered with ocean, precipitation over the global tropics can be measured satisfactorily only from space. Only a small fraction of clouds produce rain, so a space-based remote sounding technique must be able to distinguish between raining (or precipitating) clouds and non-raining clouds.

Note: Validation of these remote sounding techniques requires comparison with either rain gauge or radar measurements of precipitation. This is difficult because of:

- the different sample volumes of rain gauges and satellite instruments (10<sup>6</sup>-10<sup>8</sup> m<sup>2</sup>)
- the poor accuracy of radar measurements
- the large spatial and temporal variability of precipitation

Remote sounding "precipitation estimation" techniques can be divided into three categories.

## (1) Visible and Infrared Sounding of Rainfall

Recall that at visible and infrared wavelengths, clouds are opaque to radiation. Precipitation falling from the bottom of a cloud can be estimated from measurements of the radiation emerging from the top and/or the sides of the cloud.

This is an indirect sounding technique because the precipitation is estimated from the cloud's radiance or equivalent blackbody temperature, NOT by directly sensing the rainfall. The indirect nature of these methods makes them very specific.

e.g., approaches developed for one region may not work well for another region  
approached developed for monthly rainfall may not work for hourly rainfall

There are four further subcategories of visible and infrared sounding techniques.

### (i) Cloud indexing

This is the oldest precipitation estimation technique, and is based on the identification of cloud types in satellite images. A rain rate is assigned to each cloud type so that rainfall can be determined from observations of cloud type and cloud amount. Then the total rainfall at a particular location is simply

$$R = \sum_i r_i f_i$$

where

$r_i$  = the rain rate assigned to cloud type  $i$ , and

$f_i$  = the fraction of time that the location is covered with (or the fraction of area covered by) cloud type  $i$ .

*See figures (K&VH 9.1, 9.2) – precipitation from cloud indexing.*

### (ii) Bispectral techniques

These also use visible and infrared satellite images, making use of the fact that raining clouds are more likely to be bright in the visible (because bright clouds are thicker) and to be cold in the infrared (because cold clouds have higher cloud tops). Precipitation probabilities can be constructed for different cloud types.

*See figures (K&VH 9.7, 9.8) – 2D histograms and precipitation probabilities.*

### (iii) Life history techniques

These take into account the life cycle of a cloud, as the rain rate of a cloud is a direct function of the stage in its life cycle. This approach requires observations from GEO in order to track the cloud's evolution over time.

*See figure (K&VH 9.10) – the evolution of a typical thunderstorm.*

#### (iv) Cloud modelling

This approach incorporates cloud physics into the retrieval process, relating satellite observations to rain rates.

e.g., rain rate derived from fractional cloud cover in convective clouds

1D model relating cloud top temperature to rain rate and raining area

*See figure (K&VH 9.13) – simplified decision tree for the Schofield-Oliver technique.*

## (2) **Passive Microwave Sounding of Rainfall**

Unlike visible and infrared radiation, microwave radiation penetrates clouds. While cloud drops only interact weakly with microwave radiation, precipitation interacts very strongly with it. This allows precipitation to be directly detected with microwave radiometers.

This approach involves both scattering and absorption processes. The scattering and absorption properties of water and ice are wavelength dependent, which allows information to be retrieved from observations at different wavelengths. Specifically:

- ice scatters microwave radiation but does not absorb it
- liquid water absorbs and scatters, with absorption dominating
- scattering and absorption increase with frequency and with rain rate
- scattering by ice increases more rapidly with frequency than does scattering by water

*See figure (K&VH 9.15) – microwave scattering and absorption coefficients for water and ice.*

Based on these properties, the microwave spectrum can be divided into three regions:

- below ~22 GHz, absorption dominates
- above ~60 GHz, scattering dominates
- between 22 and 60 GHz, both absorption and scattering are important

Also, microwave radiometers observe different parts of the rain structure at different frequencies:

- below ~22 GHz, radiometers are sensitive to rain (any ice above the rain is transparent)
- above ~60 GHz, radiometers are sensitive to ice scattering (don't see rain below the ice)

Note: Microwave absorption by cloud droplets, water vapour, and oxygen may also need to be taken into account.

The Radiative Transfer Equation is used to relate rainfall rate to emission from raindrops, which is measured as brightness temperature. This allows curves of  $T_B$  vs. rainfall rate to be constructed. This approach requires a model of precipitation and the atmosphere, and thus relies on assumptions made about the atmosphere (e.g., structure of the rain layer, amount of cloud water).

*See figure (K&VH 9.16) – brightness temperature vs. rain rate for three frequencies.*

Disadvantages:

- retrieval of the rain rate requires some knowledge about the depth of the rain layer
- the contribution of cloud droplets and water vapour to the absorption may be uncertain
- poor spatial and temporal resolution of microwave radiometers – need GEO observations for good temporal coverage, but it is difficult to place a sufficiently large antenna for good spatial coverage into GEO

Methods based on the scattering of microwave radiation are promising because precipitation is the only atmospheric constituent that scatters microwave radiation. If this scattering can be detected and quantified, then it provides an unambiguous signature for precipitation.

### (3) Radar Sounding of Rainfall

Ground-based radar instruments are widely used for measuring precipitation. Short pulses (or constant waves – CW) of microwave radiation are generated by a transmitter and focussed into a narrow beam by an antenna. The power, frequency, and phase of the signal backscattered by precipitation is collected by a receiver and used to derive

- the rainfall rate (assuming a drop size distribution and fall velocity)
- drop shape
- horizontal rain speed

Terms and definitions for range-resolved (= pulsed) systems:

target range  $R = ct/2$

– is the distance between the system and the backscattering volume and is determined by the time interval,  $t$ , between transmission and reception of a pulse

direction – is determined from antenna azimuth and elevation when the pulse is received

For a ground-based radar, typically the system transmits for  $\tau \sim 1 \mu\text{sec}$ .

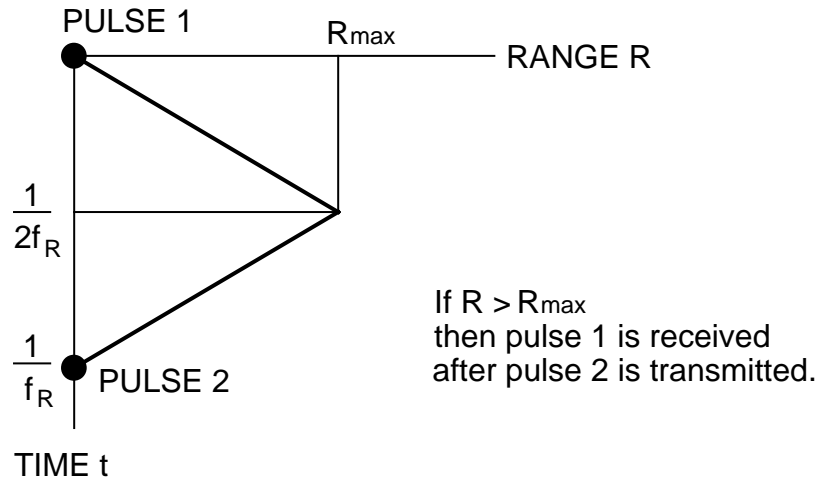
pulse length ( $h$ ) – is the finite length of the pulse, determined by how long the transmitter is on, e.g.,  $h = c \tau = 1 \mu\text{s} \times 3 \times 10^8 \text{ m/s} = 300 \text{ m}$

For a pulse of length  $h$ , the leading edge is scattered from  $R + h/2$  at the same time as the trailing edge is scattered from  $R$ . So the received signal is due to scattering from a small volume spread out in range. The resolution is this spread and is  $h/2$ .

After a pulse is transmitted, its backscattered “echo” is sampled at equally spaced time intervals to obtain information about the atmosphere at equally spaced points along the path. This is called range gating. The sampling period must be  $\geq c h/2$  for the sampled points to be independent.

pulse repetition frequency (PRF or  $f_R$ ) – number of pulses sent per second ( $\sim 100$  to  $1000$ )

unambiguous range  $R_{\max} = \text{velocity} / \text{time} = c / 2f_R$   
 – distance a pulse can travel before another pulse is transmitted



If  $R > R_{\max}$ , then the first pulse will be received after the second pulse has been transmitted, potentially leading to an incorrectly close range estimate.

*See figure (Stephens 8.3) – sampling of radar pulses.*

beam width – the angular separation between the points where the transmitted intensity is half of its maximum value

→ defined with reference to the primary lobe of the antenna pattern, which is a plot of radiated intensity vs. angular distance from the beam axis (usually has side lobes)

→ depends on wavelength and on the antenna size and shape

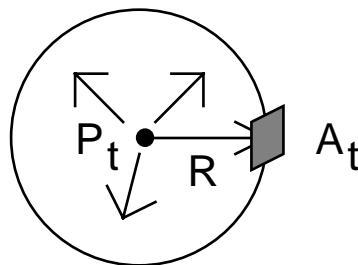
*See figure (Stephens 8.6) – cross section of the intensity pattern of a radar beam.*

### The Radar Equation

relates the received power to the transmitted power and to characteristics of the target.

Say a radar transmits at peak power  $P_t$ , which is radiated isotropically. A target of effective area  $A_t$  at range  $R$  intercepts power

$$P_{\text{intercepted}} = \frac{P_t A_t}{4\pi R^2}$$



The antenna is used to focus the energy in a narrow beam. This increases the power relative to the isotropic value such that

$$P_{\text{intercepted}} = \frac{GP_t A_t}{4\pi R^2}$$

where G is the antenna axial gain, which is a measure of the degree of focusing of the antenna.

Now, if the target area scatters the incident radiation isotropically, the power returned to an antenna of effective area  $A_e$  is

$$P_R = \frac{A_e}{4\pi R^2} P_{\text{intercepted}} = \frac{A_e}{4\pi R^2} \frac{GP_t A_t}{4\pi R^2} = \frac{GP_t A_t A_e}{(4\pi R^2)^2}$$

The gain and the antenna aperture are related by the equation:  $A_e = \frac{G\lambda^2}{4\pi}$

Thus: 
$$P_R = \frac{GP_t A_t}{(4\pi R^2)^2} \frac{G\lambda^2}{4\pi} = P_t \frac{G^2 \lambda^2}{(4\pi)^3 R^4} A_t$$

However, this assumes an isotropically scattering target. This is not generally the case, and so the target area is replaced by a radar backscatter cross section  $\sigma$  (or by  $\beta dV$  in Stephens).

$$P_R = P_t \frac{G^2 \lambda^2}{(4\pi)^3 R^4} \sigma$$

Radar equation for a single target of backscatter cross section  $\sigma$ .

Now, raindrops, snowflakes, and cloud droplets are distributed targets. They consist of many effective scattering elements that are simultaneously illuminated by a radar pulse.

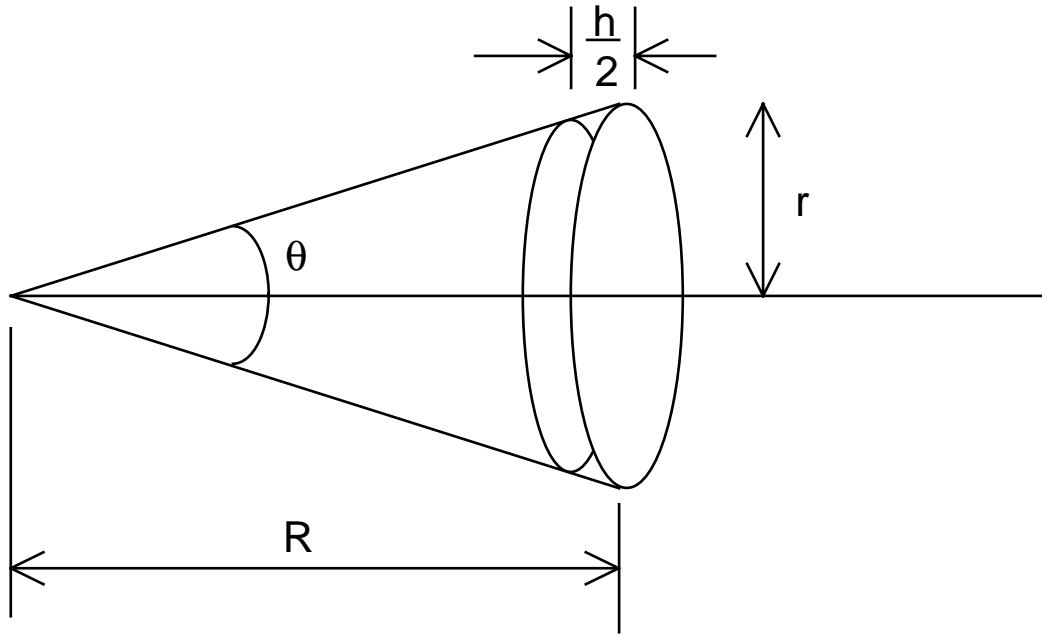
The time average of the power returned by a population of scatterers is

$$\bar{P}_R = P_t \frac{G^2 \lambda^2}{(4\pi)^3 R^4} \sum \sigma$$

where

$\sum \sigma$  = sum of the backscatter cross sections for all of the particles within the resolution volume of the radar, which is the volume that contains those particles that are simultaneously illuminated by the pulses.

The beam volume at range R is: 
$$V = \pi r^2 \frac{h}{2} \cong \pi \left( \frac{R\theta}{2} \right)^2 \frac{h}{2}$$



So the average returned power can be written as:

$$\bar{P}_R = P_t \frac{G^2 \lambda^2}{(4\pi)^3 R^4} \pi \left( \frac{R\theta}{2} \right)^2 \frac{h}{2} \eta$$

where

$\eta$  is the radar reflectivity per unit volume.

More accurately, for a Gaussian beam pattern:  $\bar{P}_R = P_t \frac{G^2 \lambda^2 \theta^2 h}{1024 \pi^2 \ln 2} \frac{\eta}{R^2}$

For radar wavelengths that are much larger than the size of the particles, Rayleigh scattering applies and the backscatter cross section for a single spherical scatterer can be shown to be:

$$\sigma = \frac{\pi^5}{\lambda^4} |K|^2 D^6$$

where

D = diameter of spherical scatterer

K = refraction term  $K = \frac{m^2 - 1}{m^2 + 2}$

$m = n - ik$  = complex index of refraction,  $n$  = refractive index,  $k$  = absorption coefficient

K depends on temperature,  $\lambda$ , and the composition of the spherical particle.

$|K|^2 \cong 0.93$  for water, 0.21 for ice

Therefore the radar cross section for ice is smaller than that for water.

Also, because of the  $\lambda^{-4}$  dependence, all things being equal,  $\sigma$  will be larger for shorter wavelengths and therefore the return signal will be stronger.

Thus, for a population of small spherical raindrops:

$$\bar{P}_R = P_t \frac{G^2 \lambda^2}{(4\pi)^3 R^4} \sum \frac{\pi^5}{\lambda^4} |K|^2 D^6 = P_t \frac{\pi^2 G^2 |K|^2}{64 \lambda^2 R^4} \sum_{\text{pulse volume}} D^6$$

This means that for small spherical scatterers, the average power received depends on only two properties of the scatterers:  $|K|^2$  and  $\sum D^6$ .

Define a new variable, the radar reflectivity factor:  $Z = \sum_{\text{unit volume}} D^6 = \int_0^{\infty} N(D) D^6 dD$

where

$N(D) dD$  = number of scatterers per unit volume with diameters in the range  $dD$ .

For raindrops,  $N(D)$  = drop size distribution.

For snowflakes,  $N(D)$  = distribution of melted diameters.

$Z$  is typically given in units of  $\text{mm}^6 \text{m}^{-3}$ .

Now combine  $P_R$  for Rayleigh scatterers, pulse volume, correction for Gaussian beam, and the reflectivity factor to get the most useful form of the radar equation for detection of precipitation:

$$\bar{P}_R = \frac{\pi^3 c}{1024 \ln 2} \left[ \frac{P_t \tau G^2 \theta^2}{\lambda^2} \right] \left[ |K|^2 \frac{Z}{R^2} \right]$$

→ first term in square brackets includes all the radar parameters

→ second term in square brackets includes all the target parameters

The received power can then be related to  $Z$  by:  $\bar{P}_R = C \frac{|K|^2}{R^2} Z$

where  $C$  is the radar constant. This is another form of the radar equation.

Because of the wide variation in  $P_R$  and  $Z$  (several orders of magnitude), this equation is sometimes written in logarithmic form.

Note: Some energy is lost from the radar beam through absorption and scattering by clouds and precipitation, and through absorption by atmospheric gases. These effects depend on wavelength and are usually worse at shorter wavelengths. Therefore, longer

wavelengths, such as 5 and 10 cm, are generally favoured for quantitative measurements of reflectivity because attenuation effects are smaller.

*See figure (Stephens 8.8) – vertical cross section of radar reflectivity.*

It is possible to relate the radar reflectivity to rainfall rate for different size distributions of raindrops. See Stephens, Sections 8.2 and 8.3 for a discussion and further details on (ground-based) radar measurements of precipitation.

## METEOROLOGICAL RADAR BANDS

BAND	$\lambda$ (cm)	$\nu$ (GHz)	SPATIAL RESOLUTION <sup>1</sup> (along the beam)	TYPICAL SMALLEST DETECTABLE PARTICLES <sup>2</sup>	SIGNIFICANT ATTENUATION BY
K	1	30	excellent	cloud droplets	cloud, rain, snow, hail
X	2	10	↓	drizzle drops	rain, intense snow, hail
C	5	6	good	rain drops <sup>3</sup>	intense rain, hail
S	10	3	↓	↓	intense hail
L	20	1.5	poor	↓	very little

- 1) Spatial resolution depends on wavelength, beam width, gain, and range.

$$\theta \approx 0.85\lambda / d_{\text{antenna}}$$

∴ larger wavelength ⇒ larger beam width ⇒ poorer spatial resolution

$$G = 4\pi A_e / \lambda^2$$

∴ larger wavelength ⇒ lower gain

A longer pulse duration  $\tau$ , giving a larger resolution volume and poorer spatial resolution is needed to produce the same returned power for larger wavelengths.

$$V = \pi \left( \frac{R\theta}{2} \right)^2 \frac{c\tau}{2}$$

∴ larger range ⇒ larger resolution volume ⇒ poorer spatial resolution

- 2) Smallest detectable particles depends on wavelength and range.

$$\sigma \propto 1/\lambda^4$$

∴ larger wavelength ⇒ smaller cross-section

so smaller particles are less "visible" to larger wavelengths

- 3) Bands C and S do not "see" clouds very well.

Difficulties with space-based precipitation radar:

- needs high power for the transmitted beam (e.g. ~300 W – 10 times too high)
- needs large antenna to provide a narrow focused beam (for good spatial resolution)
- most LEO satellites view a site twice/day, but precipitation changes rapidly (<12 hrs)
- difficult to average signals because of the speed of the satellite motion
- antenna may point in the wrong direction for the return signal (also due to the speed)

Only one space-based precipitation-sensing radar instrument has been launched

→ TRMM = Tropical Rainfall Measuring Mission

- launched in 1997 by NASA and NASDA with a planned mission life of three years
- 350-km circular orbit with a 35° inclination angle
- main objective is to measure rainfall and energy (i.e. latent heat of condensation) exchange in the tropical and subtropical regions of the world
- the primary rainfall instruments are the TRMM Microwave Imager (TMI), the precipitation radar (PR), and the Visible and Infrared Radiometer System (VIRS)
- also carries two related EOS instruments in the Clouds and Earth's Radiant Energy System (CERES) and the Lightning Imaging System (LIS)

TMI is a nine-channel passive microwave radiometer that will measure brightness temperatures to sound to different depths in a precipitating cloud. PR provides specific height information based upon the time delay of the precipitation-backscattered return power. VIRS adds cloud-top temperatures and structures.

*See figure (Kummerow et al. Fig. 1) – schematic view of scan geometries.*

Scientific goals of the TRMM Precipitation Radar

- to provide 3D structure of rainfall, particularly of the vertical distribution
- to obtain quantitative rainfall measurements over land as well as over ocean e.g., intensity and distribution of rain, rain type, storm depth, the height at which snow melts into rain, latent heat released
- to improve the overall TRMM precipitation retrieval accuracy by combined use of active (PR) and passive (TMI and VIRS) sensor data

*See figures – TRMM precipitation measurements.*

## TRMM PR Characteristics

Frequency	13.796, 13.802 GHz
Rain rate sensitivity	0.7 mm/hour
Swath width	215 km
Observable range	Surface to 15 km altitude
Horizontal resolution	4.3 km (nadir)
Vertical resolution	0.25 km (nadir)
Antenna	
Type	128-element active phased array system
Beam width	0.71° x 0.71°
Aperture	2.0 m x 2.0 m
Scan angle	± 17° (Cross track scan)
Transmitter/receiver	
Type	SSPA & LNA (128 channels.)
Peak power	500 W (at antenna input)
Mean power	224 W
Pulse width	1.6 s x 2 ch. (Transmitted pulse)
PRF	2776 Hz
Dynamic range	70 dB
Number of indep. samples	64
Data rate	93.2 kbps
Size of mechanical structure	2.3 m x 2.3 m x 0.7 m
Geophysical data products	3D rain-rate maps, qualitative rain characteristics (rain type, storm top, and brightband heights), and statistics of surface scattering cross sections from nadir to 17° incidence angles

## 5.4 Measurements of Winds

### *References*

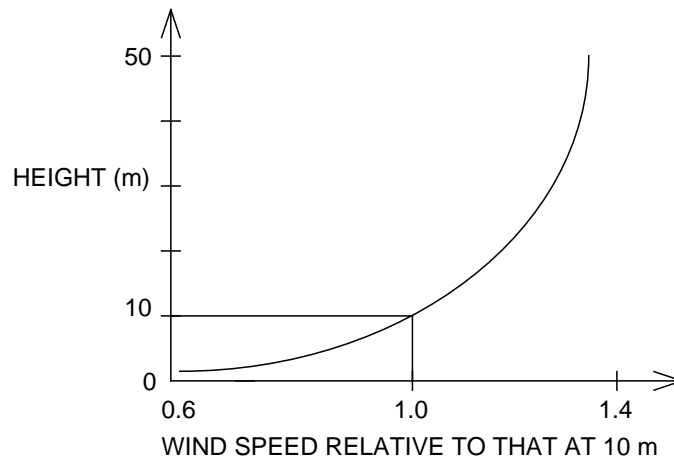
- *Kidder and Vonder Haar: chapter 7*
- *Stephens: chapter 8, pp. 438-454*
- *Houghton, Taylor, and Rodgers: chapter 12, pp. 227-232*

Winds are generally caused by imbalances in the atmosphere due to variations in temperature and pressure. Air moves in an attempt to reach equilibrium, but solar heating prevents equilibrium from being attained. Air movement is three-dimensional, and so both the vertical and the horizontal components are needed in order to fully define the dynamical state of the atmosphere.

Vertical motion occurs on a small scale near the ground (due to eddies caused by turbulent flow and convection), and on a large scale (due to solar heating in the tropics) which drives the general circulation of the atmosphere.

*See figure – middle atmosphere dynamics.*

Wind speed increases rapidly with height up to ~100 m above the surface, but becomes roughly constant at some height between 500 and 2000 m, as the effect of the surface (e.g., friction) becomes negligible. This region in which the surface influences the wind is the planetary boundary layer (PBL). Above the PBL, the wind speed becomes constant and equal to the geostrophic wind, which is the wind that blows parallel to the isobars.



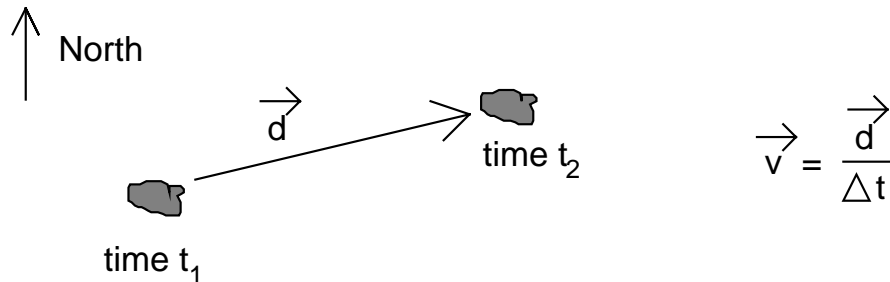
Winds are an important parameter in defining the current state of the atmosphere and in predicting its future behaviour.

In situ wind measurements are made using ground-based manual and automated wind vanes, wind direction sensors, and anemometers (cup, propeller, pressure, vortex, thermal). Wind speed and direction can be measured up into the stratosphere by radar or GPS tracking of radiosondes.

Techniques for measuring winds from space can be divided into four categories.

### (1) Winds from Cloud and Vapour Tracking

Imagers on geostationary satellites provide frequent images of the same area which can be used to track the movement of clouds. The vector difference of the location of a cloud in two images divided by the time interval gives an estimate of the horizontal wind at the level of the cloud. Winds obtained in this way are called cloud-track or cloud-drift winds.



This method can be performed

- manually using a cursor to mark appropriate clouds – accurate but tedious
- automatically using cross correlation between images – faster, easier, but less accurate

This approach can only be applied to obtain winds when clouds are present, and is unable to provide low-level winds when thick cloud cover is present (e.g., hurricanes).

It is most useful for determining

- winds at low levels using small (0.5 to 4 km diameter) convective cumulus clouds at ~900 mbar
- winds at upper levels using cirrus clouds at ~200 mbar in the troposphere.

Otherwise it is difficult to determine cloud heights without more information.

Typically, wind speeds obtained using different satellites have rms differences of 4 m/s (for low-level winds) to 6 m/s (for high-level winds), while cloud track winds differ by 5-6 m/s (low levels) to 10-15 m/s (high levels) compared to radiosonde winds. These latter differences are due to errors in the height assignment of the cloud track winds, poor collocation in time or space, and errors in measurement and tracking.

*See figure (K&VH 7.1) – SMS 2 visible image and low-level winds derived by cloud tracking.*

Images in the 6.7  $\mu\text{m}$  water vapour channel can also be used for tracking

→ vapour-track winds can be estimated in cloud-free areas.

The weighting function of the water vapour channel peaks at 450 mbar so this approach is useful for determining winds in the mid-troposphere where there are few clouds. However, it is still difficult to assign accurate cloud heights. Water vapour images can be fuzzier than cloud images, making it more difficult to track specific features.

## (2) Winds from Soundings

At latitudes outside the tropics ( $\geq 10^\circ$ ), the wind field can be related to the density field. Given temperature soundings and sea-level pressure, the height of other pressure surfaces can be determined. Three relationships can then be used to derive winds for these heights.

- geostrophic wind – blows parallel to isobars (horizontally) due to the balance between the pressure gradient force and the Coriolis force (arises from motion in a rotating reference frame)

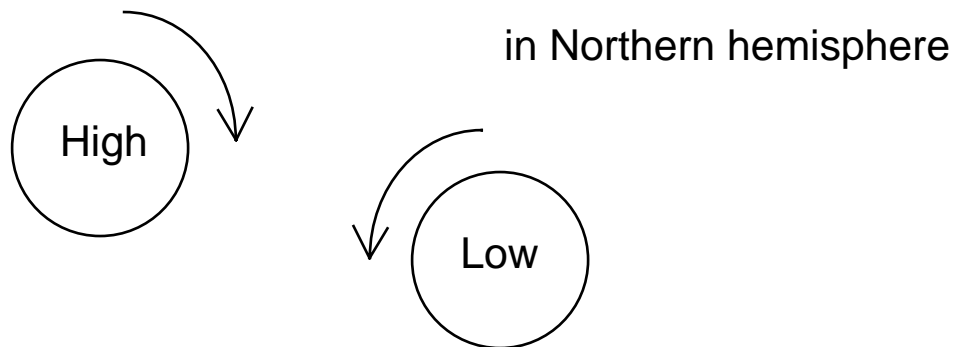
$$\vec{v}_g = \frac{1}{f} \hat{k} \times \nabla \bar{\Phi}$$

where

$$f = 2 \frac{d\bar{\Omega}_E}{dt} \sin \theta = \text{Coriolis parameter, with } \frac{d\bar{\Omega}_E}{dt} = \text{angular velocity of Earth, } \theta = \text{latitude}$$

$\hat{k}$  = unit vector is the vertical

$\bar{\Phi} = gz = \text{geopotential}$



- gradient wind – also blows parallel to isobars but is a better approximation than the geostrophic wind when the motion has large curvature (includes an acceleration term to allow for curvature)

$$v_{gr} = \frac{2v_g}{1 + \sqrt{1 + 4v_g / fR_T}}$$

where

$R_T$  = radius of curvature of the trajectory of an air parcel

- quasi-geostrophic wind – more accurate calculation of the wind field in three dimensions

After using temperature soundings and sea-level pressure to derive the heights of higher pressure surfaces, these three winds can be calculated. In one study, comparisons with radiosonde data found that the best agreement with the radiosondes was obtained with the gradient wind estimate (rms error < 10 m/s at 300 mbar). Results were worse near the surface, where satellite soundings are less accurate.

### (3) Ocean Surface Winds

These have been derived using four approaches:

#### (i) Scatterometers (active microwave radar)

- measure backscattering cross section per unit sea surface area ( $\sigma^0$ , unitless)
- wind gives rise to waves of all wavelengths on the sea surface – waves of  $\lambda$  near that of the radar will backscatter via Bragg scattering
- $\sigma^0$  can be related to the surface wind speed and direction, although this is a complex relationship as  $\sigma^0$  also varies with water temperature, viscosity, surface tension, etc.
- the largest backscatter is in the upwind and downwind directions

e.g., Seasat-A Satellite Scatterometer (SASS), 1978 – measured  $\sigma^0$  at 2 cm

→ observed each ocean spot twice from different azimuth angles in order to derive wind speed and direction

→ designed to retrieve wind speed at 2 m/s accuracy and direction at 20° accuracy

#### (ii) Passive microwave emission

- is a function of wind speed over the sea surface (although can't determine the wind direction)
- wind-induced waves and foam change emittance (as well as backscatter) for non-nadir viewing
- foam forms on the surface at wind speeds above ~7 m/s, and covers more area as the speed increases → since foam is essentially black, the emittance increases rapidly (almost linearly) with wind speed above 7 m/s

e.g., Seasat-A Scanning Multichannel Microwave Radiometer (SMMR)

→ wind speeds obtained to 2.7 m/s accuracy using regression of brightness temperature against observed winds

#### (iii) Dvorak technique for tropical cyclone winds

- uses visible and IR images of tropical cyclones to classify them as one of eight types
- the cyclone intensity and wind speed can then be derived from the cyclone type
- although subjective, this approach is widely used and gives good wind estimates
- also possible to use the equivalent blackbody temperature at the eye and at the edge of the cyclone to determine its strength

#### (iv) Microwave sounding of tropical cyclone winds

- can probe the cloudy interior of cyclones since they are unaffected by clouds
- the centre of a cyclone is warmer than the edges and results in a surface pressure drop
- the brightness temperature can be measured in the microwave, and its radial gradient can be correlated with the surface pressure gradient and hence to the wind speed at the outer edge of the cyclone
- typical accuracies are 6 m/s in wind speed

#### **(4) Doppler Wind Measurements**

This approach has been used by the WINDII (Wind Imaging Interferometer) and HRDI (High Resolution Doppler Imager) on UARS.

The atmospheric limb is viewed and the Doppler shift in visible/near IR absorption and emission lines of O, O<sub>2</sub>, and OH is measured. This Doppler shift can be related to the relative velocity between the satellite and the volume of air being sampled. By observing the same location as UARS approaches and leaves an area, both the speed and direction of the horizontal wind can be determined.

#### **WINDII**

- operating on UARS since 1991
- developed by Gordon Shepherd, York University (Principal Investigator)
- measures the horizontal wind to  $\pm 10$  m/s accuracy and temperature from 80 to 300 km
- measures the Doppler widths and shifts of isolated spectral lines emitted by the airglow and aurora in the mesosphere and the lower thermosphere (O at 557.7 nm, O<sub>2</sub> at 762.0 nm, and OH at 730.0 nm)

The three principal objectives for the WINDII experiment were:

- 1) To measure two-dimensional vertical profiles of the horizontal wind velocity and Doppler temperature of the neutral atmosphere in the altitude range of 70 to 315 km, and to determine these profiles as a function of latitude, time of day, and time of year.
- 2) To measure the global distribution of small-scale wave-like structures, down to a scale size of 3 km.
- 3) To study dynamic and thermal aspects of the neutral atmospheric energy balance in the observed altitude range.

Note: The mesosphere/lower thermosphere is a region of complex dynamics where atomic oxygen is generated, upward propagating gravity induced waves become important, and the transition from a mixed atmosphere to the region of diffusive equilibrium occurs.

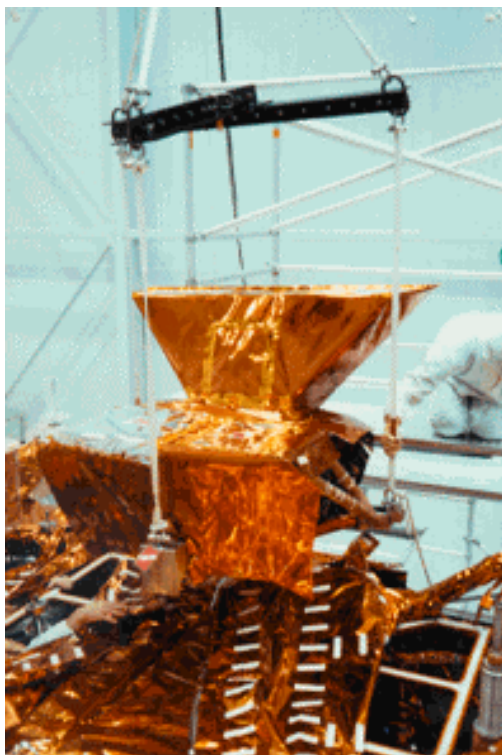
The WINDII instrument

- has two fields-of-view, at 45° and 135° from the spacecraft velocity vector, so that each region of the atmosphere is imaged twice (7 minutes apart), providing both horizontal components of the neutral wind
- uses an imaging CCD camera (320 by 256 pixels) that views the limb through a field-widened Michelson interferometer
- takes four images, with the interferometer optical path difference changed by 1/4 wavelength between images
- interference filters are used to isolate specific spectral lines

These images can be analysed to provide fringe phase (leading to wind velocity), fringe modulation depth (leading to temperature), and emission rate.

*See WINDII figures.*

<b>WIND Imaging Interferometer (WINDII)</b>	
Type of measurement	Doppler shift and line broadening of atmospheric emission in the visible and near infrared
Type of instrument	Field-widened Michelson interferometer
Geophysical measurements	Atmospheric temperature and horizontal wind vector
Wavelength coverage	550 to 780 nm
Viewing geometry	45°, 135° to spacecraft velocity vector. Maximum latitude sampled is 74°
Comments	Orthogonal measurements for same atmospheric volume separated in time by approximately 8 minutes
Vertical FOV	6°, 70 to 315 km at the horizon
Vertical resolution	4 km at horizon (nominal); 1.5 km at horizon (potential)
Horizontal resolution	20 km (along track) at horizon
Time required for measurement	Time required to perform measurement is 8 sec. Distance along spacecraft track 60.5 km
Instrument weight	269 lb
Average power	73 watts
Data rate	2.0 kbps



## HRDI

- also operating on UARS since 1991
- measures the horizontal wind to better than 5 m/s over prescribed regions of the atmosphere extending from the upper troposphere through the thermosphere
  - stratospheric altitude range of 10-40 km
  - mesosphere and lower thermosphere (MLT) altitude range of 50-115 km
- the first satellite instrument capable of performing direct global-scale measurements of the stratospheric wind field
- measures the Doppler shift of absorption and emission lines of O<sub>2</sub>
- also obtains temperatures and volume emission rates in the MLT, and cloud top heights, effective albedos, aerosol phase functions, and scattering coefficients in the stratosphere

### The HRDI instrument

- high-resolution triple-etalon Fabry-Perot interferometer that views the Earth's atmosphere through a telescope
- spatially scans the interference fringe plane with a multichannel array detector to perform wavelength analysis on the light detected from atmospheric emission or absorption features

*See HRDI figures.*

<b>High Resolution Doppler Imager (HRDI)</b>	
Type of measurement	Doppler shift and line broadening of scattered sunlight and atmospheric emission in the visible wavelengths
Type of instrument	Triple-etalon Fabry-Perot interferometer
Geophysical measurements	Horizontal-vector wind and atmospheric temperature
Wavelength coverage	400 to 800 nm
Viewing geometry	45°, 135°, 225°, 315° ± 5° to spacecraft velocity vector
Maximum latitude	74°
Comments	Gimballed telescope can view any azimuth direction; orthogonal measurements for same sample volume separated by ~8 min.
Spectral resolution	0.001 nm
Vertical resolution	6 km at limb (0.12° FOV)
Horizontal resolution	80 km at limb (1.7° FOV)
Time required for vertical scan	7.33 sec for one 90 km scan
Distance along spacecraft track	55 km per scan. Potential for four vertical scans of vector wind in 500 km along track
Instrument weight	348 lb
Average power	109 watts
Data rate	4.750 kbps